

# Gryffin: An algorithm for Bayesian optimization for categorical variables informed by physical intuition with applications to chemistry

Florian Häse,<sup>1,2,3,4,\*</sup> Loïc M. Roch,<sup>2,3,4,5</sup> and Alán Aspuru-Guzik<sup>2,3,4,6,†</sup>

<sup>1</sup>*Department of Chemistry and Chemical Biology,  
Harvard University, Cambridge, Massachusetts, 02138, USA*

<sup>2</sup>*Vector Institute for Artificial Intelligence, Toronto, ON M5S 1M1, Canada*

<sup>3</sup>*Department of Computer Science, University of Toronto, Toronto, ON M5S 3H6, Canada*

<sup>4</sup>*Department of Chemistry, University of Toronto, Toronto, ON M5S 3H6, Canada*

<sup>5</sup>*ChemOS Sàrl, 1006 Lausanne, VD, Switzerland*

<sup>6</sup>*Lebovic Fellow, Canadian Institute for Advanced Research, Toronto, Ontario M5G 1Z8, Canada*

(Dated: March 30, 2020)

Designing functional molecules and advanced materials requires complex interdependent design choices: tuning continuous process parameters such as temperatures or flow rates, while simultaneously selecting categorical variables like catalysts or solvents. To date, the development of data-driven experiment planning strategies for autonomous experimentation has largely focused on continuous process parameters despite the urge to devise efficient strategies for the selection of categorical variables to substantially accelerate scientific discovery. We introduce GRYFFIN, as a general purpose optimization framework for the autonomous selection of categorical variables driven by expert knowledge. GRYFFIN augments Bayesian optimization with kernel density estimation using smooth approximations to categorical distributions. Leveraging domain knowledge from physico-chemical descriptors to characterize categorical options, GRYFFIN can significantly accelerate the search for promising molecules and materials. GRYFFIN can further highlight relevant correlations between the provided descriptors to inspire physical insights and foster scientific intuition. In addition to comprehensive benchmarks, we demonstrate the capabilities and performance of GRYFFIN on three examples in materials science and chemistry: (i) the discovery of non-fullerene acceptors for organic solar cells, (ii) the design of hybrid organic-inorganic perovskites for light-harvesting, and (iii) the identification of ligands and process parameters for Suzuki-Miyaura reactions. Our observations suggest that GRYFFIN, in its simplest form without descriptors, constitutes a competitive categorical optimizer compared to state-of-the-art approaches. However, when leveraging domain knowledge provided *via* descriptors, GRYFFIN can optimize at considerable higher rates and refine this domain knowledge to spark scientific understanding.

## I. INTRODUCTION

The discovery of functional molecules and advanced materials is recognized as one of the fundamental obstacles to the development of emerging and future technologies to face immediate challenges in clean energy, sustainability and global health.<sup>1,2</sup> To date, accelerations of scientific discovery workflows across chemistry, materials science and biology have largely been driven by combinatorial high-throughput strategies with automated experimentation equipment.<sup>3–7</sup> Despite remarkable successes with high-throughput approaches,<sup>8–12</sup> the combinatorial explosion of molecular and materials candidates renders exhaustive evaluations on large scales impossible. This limitation can be alleviated by adaptive search strategies which selectively explore the search space and only evaluate the most promising materials candidates.<sup>13</sup> Autonomous platforms have been suggested as a next-generation approach to experimentation for accelerated scientific discovery.<sup>14–17</sup> These platforms augment automated experimentation systems with data-driven algo-

rithmic strategies to continuously plan new experiments inspired by previously collected measurements.

Recently, data-driven experiment planning has experienced increased attention by the scientific community across various applications including the search for antimicrobial peptides,<sup>18</sup> the synthesis of organic molecules,<sup>19,20</sup> the discovery and crystallization of polyoxometalates,<sup>21</sup> the discovery of metallic glasses,<sup>22</sup> the optimization of carbon dioxide-assisted nanoparticle deposition,<sup>23</sup> and the creation of Bose-Einstein condensates.<sup>24</sup> Motivated by the successes of data-driven experiment planning, the development and deployment of autonomous workflows for scientific discovery as well as their benefits over conventional experimentation strategies are being actively explored.<sup>25</sup> For example, autonomous platforms have been reported for the optimization of reaction conditions in the context of flow chemistry,<sup>26–28</sup> the unsupervised growth of carbon nanotubes,<sup>29,30</sup> autonomous synchrotron X-ray characterization,<sup>31,32</sup> the discovery of thin-film materials,<sup>33</sup> the synthesis of inorganic photoluminescent quantum dots,<sup>34</sup> and the discovery of photostable quaternary polymer blends for organic photovoltaics.<sup>35</sup>

Although autonomous experimentation platforms appear to be on the rise, and data-driven approaches are emerging as viable experiment planning strategies, the

\*Electronic address: hase.florian@gmail.com

†Electronic address: alan@aspuru.com

forementioned examples mostly targeted experimentation tasks with continuous process parameters. Yet, scientific discovery in chemistry and materials science typically involves the simultaneous optimization of continuous and categorical variables such as the selection of a catalyst or solvent, which cannot be targeted efficiently with continuous optimization methods. Approaches to the data-driven selection of categorical parameters are often handcrafted and involve human decisions which can adversely affect the experimentation throughput. Examples of experimentation workflows involving the selection of categorical variables with partial human interaction have been demonstrated in the context reaction optimization for flow chemistry.<sup>36–38</sup> The lack of a general purpose approach to the data-driven optimization of categorical variables is a challenge to autonomous discovery workflows and appears as a major obstacle to the massive deployment of autonomous experimentation platforms.

The machine learning community is actively exploring algorithmic approaches to the data-driven selection of categorical variables in the context of hyperparameter optimization,<sup>39</sup> or control parameters in robotics.<sup>40</sup> Yet, these applications are different from optimization tasks in chemistry and materials science where categorical variables can usually be characterized by a notion of similarity between individual choices. For example, co-polymers for hydrogen production can be synthesized from categorical monomers which differ in their reactivity.<sup>41</sup> More generally, similarity measures between molecules and materials can be introduced based on their physical, chemical and structural properties. An experiment planning strategy which actively leverages physicochemical descriptors of candidate materials would be most desirable to (i) accelerate scientific discovery and (ii) gain scientific insights to inspire the design of even more promising molecules and materials which are not included in the search library.

In this work we introduce GRYFFIN, a global optimization strategy for the selection of categorical variables in autonomous workflows. GRYFFIN implements an efficient Bayesian optimization framework leveraging kernel density estimation directly on the categorical space, which can be accelerated with domain knowledge in the form of physicochemical descriptors by locally redefining the metric on the categorical space. In addition, GRYFFIN can construct more informative descriptors on-the-fly to highlight the relevance of some of the provided descriptors and inspire scientific interpretations while identifying desired categorical options at a faster rate.

We highlight the applicability and performance of GRYFFIN on a set of synthetic benchmark functions and three real-world tasks: the discovery of small molecule non-fullerene acceptors for organic solar cells, the discovery of hybrid organic-inorganic perovskites for light-harvesting and the combined selection of ligands and optimization of process parameters for Suzuki-Miyaura coupling reactions. We identify three key advantages of GRYFFIN over state-of-the-art approaches to categorical

optimization: (i) it provides a competitive framework for the descriptor-less optimization of categorical variables, (ii) can optimize at significantly higher rates with provided and refined descriptors which can inspire scientific insights, and (iii) integrates with continuous optimization strategies to enable the robust and efficient optimization of mixed continuous-categorical domains for sequential and batched workflows.

## II. BACKGROUND AND RELATED WORK

Experiment planning can be formulated as an optimization task, where we consider a set of controllable parameters within a defined domain,  $\mathbf{z} \in \mathcal{Z}^n$ , and an experimental response,  $f(\mathbf{z})$ , for each of the parameter choices within the domain. In the context of reaction optimization, the controllable parameter could for example include the reaction temperature, the amount of solvent, and the choice of the catalyst, while the experimental response could be quantified via the rate at which the desired product is generated. The optimization domain is also referred to as the *design space* or the *candidate space*. The optimization task in experiment planning consists in the identification of specific parameter values,  $\mathbf{z}^* \in \mathcal{Z}^n$ , which yield the desired experimental outcome,  $f(\mathbf{z}^*)$ . For simplicity, we will consider minimization tasks from hereon, i.e. we formulate  $f$  such that  $\mathbf{z}^* = \underset{\mathbf{z} \in \mathcal{Z}}{\operatorname{argmin}} f(\mathbf{z})$  corresponds to the desired experimental result. The optimization task can be approached with a closed-loop strategy, which iteratively evaluates a set of options  $\mathbf{z}_j$  and records to associated responses,  $f_j = f(\mathbf{z}_j)$ , to gradually collect a set of observations,  $\mathcal{D}_n = \{\mathbf{z}_j, f_j\}_{j=1}^n$ , as feedback to the experiment planning strategy.

The optimization of categorical parameters poses additional challenges compared to the optimization of continuous or discrete variables due to the lack of a natural ordering between individual parameter values, which is illustrated in the supplementary information (see Sec. S.2). Regardless of the optimization strategy, the confidence of having identified the best performing candidate in the search space increases with the number of evaluated candidates. In the best case, only one evaluation is required, while in the worst case all candidates in the search space need to be evaluated. Yet, the choice of the optimization strategy modulates the chance of having identified the best performing candidate after a certain number of evaluations and consequently the average fraction of the candidate space that needs to be evaluated to identify the most desired one.

Straightforward search strategies rely on exhaustive random<sup>42–44</sup> or systematic<sup>45–47</sup> evaluations of all candidates without leveraging any feedback from collected responses to refine the search policy. In the absence of accurate prior expectations on the performance of individual candidates, both random and systematic search

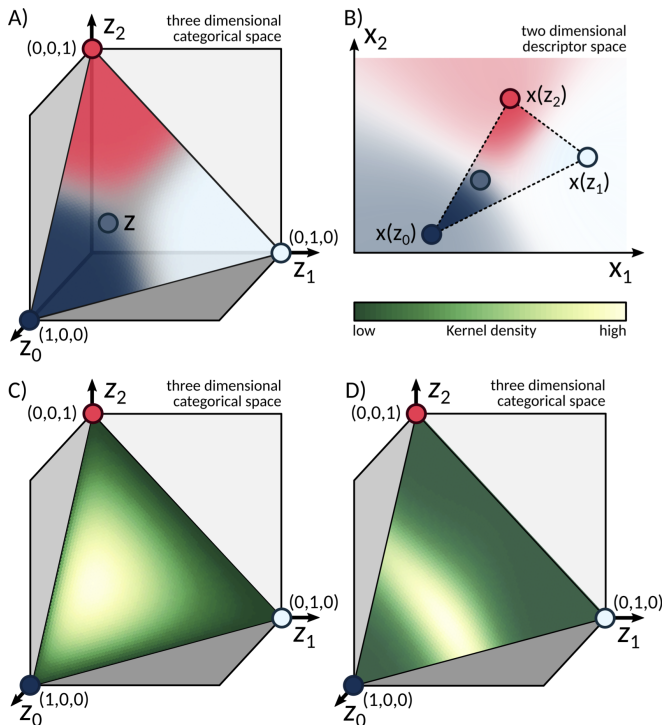


FIG. 1: Illustrations of the naïve and the static GRYFFIN strategies for the (descriptor-guided) optimization of categorical variables. (A) Illustration of a categorical variable with three options represented on a simplex. Color contours indicate the affiliation of any given point on the simplex to one of the categorical options at the corners. (B) Representation of a continuous descriptor space, where descriptors are associated with the categorical options shown in panel A. Color contours indicate the affiliation with individual options of the categorical variable. (C) Illustration of a generic kernel density on the simplex modeled with a concrete distribution. (D) Illustration of a descriptor-guided transformation of the kernel density shown in panel C based on the descriptors shown in panel D.

strategies require the evaluation of 50 % of all candidates, on average, to identify the best performing candidate and are therefore only applicable to relatively small search spaces. Yet, exhaustive strategies are massively parallelizable and thus well suited for high-throughput experimentation. Genetic algorithms and evolutionary strategies<sup>48–50</sup> extend the idea of a random exploration of the search space, but condition their exploration policies on a population of candidate solutions which have already been evaluated. In contrast to a globally random exploration, new candidates are selected based on local perturbations on the population of the best performing candidates. During the optimization, the better performing candidates substitute the poorly performing candidates.<sup>51</sup>

Bayesian optimization<sup>52,53</sup> has recently gained increased attention as a competitive global optimization strategy across various fields,<sup>54,55</sup> including automatic machine learning,<sup>56–58</sup> and experimental design.<sup>59–61</sup> The

common framework of Bayesian optimization strategies follows two basic steps: (i) the construction of a surrogate to the unknown response surface from a probabilistic model based on collected measurements, and (ii) the selection of new candidates with an acquisition function which balances the expected performance of each candidate and the uncertainty on this estimate as determined by the surrogate. Different probabilistic models have been suggested to construct the surrogate, including Gaussian processes,<sup>62</sup> random forests<sup>63</sup>, and Bayesian neural networks,<sup>64</sup> and different acquisitions functions such as probability of improvement,<sup>53</sup> expected improvement,<sup>65</sup> upper (lower) confidence bound<sup>66</sup> predictive entropy,<sup>67</sup> and kernel density based formulations,<sup>68</sup> are commonly employed.

Extensions of Bayesian optimization frameworks to categorical parameter domains are under active development. One approach consists in the representation of categorical parameters as one-hot encoded vectors.<sup>39,69,70</sup> This representation expresses the  $j$ -th option of a categorical variable  $\mathbf{z}$  with  $n$  different options,  $\mathbf{z} = \{z_1, \dots, z_n\}$ , as an  $n$ -dimensional vector with elements  $z_i = \delta_{ij}$  for  $1 \leq i \leq n$ , which can be interpreted as the corners of an  $n$ -dimensional simplex,  $\mathbf{z} \in \Delta^{n-1} = \{\mathbf{z} \in \mathbb{R}^n | z_i \in [0, 1] \text{ and } \sum_{i=1}^n z_i = 1\}$  (see Fig. 1a). Standard Bayesian optimization strategies for continuous parameter domains can be deployed on these one-hot encoded categorical variables, such that even optimizations of mixed continuous-categorical domains are possible. However, the most promising choices for future evaluations are determined by projecting promising candidates from the continuous space to the one-hot boundaries. This strategy presents two limitations: (i) redundancies in the projection arise from the fact that the continuous optimization space contains an additional degree of freedom compared to the categorical domain, and (ii) the one-hot encoding imposes an equal measure of covariance between all choices of the categorical variables such that we cannot account for imbalanced similarities.

Redundancies in the projection can be reduced by imposing constraints on the acquisition function on the continuous domain. For example, the acquisition function can be modified such that covariances are computed after the projection operation.<sup>71,72</sup> This modification results in a stepwise defined acquisition function from which choices for future evaluations can be suggested directly. However, stepwise functions are generally more challenging to optimize than smooth functions, and this modification still retains equal covariance measures between individual choices of categorical variables.

### III. FORMULATING GRYFFIN

Building upon previous works (see Sec. II) we base the formulation of GRYFFIN on a one-hot encoding of categorical variables. Rather than constructing the surrogate on the continuous space spanned by the one-hot encoded

categorical choices where each dimension is bounded by  $[0, 1]$ , GRYFFIN aims to support the surrogate on the simplex to avoid projection redundancies. To this end we model categorical parameters as random variables and extend the recently reported PHOENICS approach<sup>68</sup> from continuous domains to categorical domains to construct the surrogate from reweighted kernel density estimates for the categorical parameters. Beyond the implementation of kernel density based Bayesian optimization on categorical domains, we further demonstrate how physical and chemical domain knowledge can be used to transform the surrogate to accelerate the search and how this bias can be refined during the optimization to identify and interpret relevant domain knowledge.

### A. Categorical optimization with naïve Gryffin

Naïve GRYFFIN constructs kernel densities by extending the one-hot encoding of categorical options to the entire simplex, i.e. we consider  $\mathbf{z} \in \Delta^{n-1}$ . The largest entry of any given point  $\mathbf{z}$  can be used to associate this point to a realizable option  $\zeta$  (see Fig. 1a). Various probability distributions with support on the simplex have been introduced in the past. The Dirichlet distribution, for example, constitutes the conjugate prior to the categorical distribution.<sup>73</sup> Another example is the logistic normal distribution which ensures that the logit of generated samples follow a standard normal distribution.<sup>74</sup> While both of these distributions are widely used, their deployment in a computational graph is numerically involved due to demanding inference and sampling steps. Directed probabilistic models can be implemented at low computational cost if stochastic nodes of such graphs can be reparameterized into deterministic functions of their parameters and stationary noise distributions.<sup>75</sup> Such reparameterizations, however, are unknown for the Dirichlet and the logistic normal distribution.

The recently introduced concrete distribution<sup>76</sup> (simultaneously introduced as Gumbel-Softmax),<sup>77</sup> illustrated in Fig. 1c, overcomes this obstacle. This distribution is supported on the simplex and parameterized by a set of deterministic variables with noise generated from stationary sources. As such, the concrete distribution is amenable to automatic differentiation frameworks for accelerated sampling and inference. In addition, the concrete distribution contains a temperature parameter,  $\tau$ , which can be tuned to smoothly interpolate between the discrete categorical distribution and a uniform distribution on the simplex. As such, this temperature parameter controls the localization of constructed kernel densities towards the corners of the simplex.

Naïve GRYFFIN estimates kernel densities from concrete distributions and conditions the parameters of the concrete distribution on the sampled candidates as suggested in the PHOENICS framework. The temperature parameter is modified based on the number  $n$  of collected observations,  $\tau \sim n^{-1}$ , such that the priors gradually

transition from a uniform distribution to a continuous approximation of the categorical distribution. Options for future evaluation are determined via the acquisition function of PHOENICS, which compares the constructed kernel densities to the uniform distribution on the simplex. Using a sampling parameter  $\lambda$  to reweight the uniform distribution, this acquisition function can favor a bias towards exploration or exploitation explicitly and natively enable batch optimization. Details of this procedure are provided in the supplementary information (see Sec. S.1.A).

The computational cost of the algorithm can further be reduced significantly by introducing an approximation to the computation of the kernel densities. The approximation is based on the idea that the low density regions of the kernel densities indicate a lack of information. A precise estimate of the kernel densities in these regions might therefore not be required. We find that an approximate estimate of the kernel densities in low density regions can significantly accelerate the computation without requiring additional evaluations. Details on this approximation are provided in the supplementary information (see Sec. S.3.A)

### B. Descriptor-guided searches with static Gryffin

The naïve GRYFFIN approach imposes an equal measure of covariance between individual options of categorical variables, which is undesired in cases where a notion of similarity can be established between any two given options. Especially in the context of scientific discovery, similarities between the options of categorical variables can be defined, for example, *via* physico-chemical descriptors for small molecules or material candidates. We extend the naïve approach by assuming that the metric to measure similarity between any two options is based on the Euclidean distance between real-valued  $d$ -dimensional descriptor vectors,  $\mathbf{x} \in \mathbb{R}^d$ , which are uniquely associated with individual categorical options (see Fig. 1a,b).

While the descriptors are embedded in a continuous space, their arrangement in this space is unknown for a generic optimization task and only selected points in the descriptor space can be associated with realizable categorical options. These limitations present major obstacles to optimization strategies which operate directly on the descriptor space. Instead, we propose to leverage the naïve GRYFFIN framework but redefine the metric on the simplex based on the provided descriptors. Following this strategy, the length of an infinitesimal line element on the simplex is conditioned not only on the corresponding infinitesimal change of location on the simplex, but also on the infinitesimal change of the associated descriptors. Imposing a linear mapping between points on the simplex  $\mathbf{z}$  and the descriptor space  $\mathbf{x}$ , we can compute the length of a finite line element,  $\Delta s$ , following the redefined



metric to be

$$\Delta s^2 = \sum_{m=1}^{\#descs} \sum_{i,j=1}^{\#opts} \left( x_m^i - \sum_{k=1}^{\#opts} z_k x_m^k \right)^2, \quad (1)$$

which is derived in detail in the supplementary information (see Sec. S.1.B). Kernel densities generated by the naïve approach can be transformed following this descriptor-based definition of distances on the simplex to reflect the similarity between individual options as illustrated in Fig. 1a,b. As a consequence, the evaluation of one option of the categorical variable will be more informative with respect to the expected performance of other, similar options. Further implications of imposing a descriptor-guided metric on the simplex are illustrated in the supplementary information (see Sec. S.1.B).

We refer to the descriptor-guided categorical optimization as static GRYFFIN, as user-provided descriptors are used without further modifications. The benefits of static GRYFFIN over naïve GRYFFIN with respect to an accelerated search could depend on the provided descriptors: more informative descriptors are expected to efficiently guide the algorithm to the best performing options, while less informative descriptors have the potential to mislead the algorithm. These possibilities are empirically explored in more detail in Sec. IV.

### C. Descriptor refinement with dynamic Gryffin

The dynamic formulation of GRYFFIN aims to alleviate the expected sensitivity of the performance of static GRYFFIN on the choice of provided descriptors by transforming them during the optimization. Specifically, dynamic GRYFFIN infers a transformation,  $T$ , which constructs a new set of descriptors,  $\mathbf{x}'$ , from the provided descriptors,  $\mathbf{x}$ , based on the feedback collected from evaluated options. The transformation  $T$  can be constructed to target two major goals: (i) the generation of more informative descriptors,  $\mathbf{x}'$ , which help to navigate the candidate space more efficiently, and (ii) the interpretable identification of relevant domain knowledge to inspire design choices and scientific insights as we will demonstrate in Sec. V. In addition to these two goals, the transformation  $T$  is required to be robust with respect to overfitting due to the low data scenarios which are commonly encountered in autonomous workflows.

In an attempt to balance flexibility, robustness and interpretability, we suggest to construct this transformation  $T$  from a learnable combination of the provided descriptors

$$\mathbf{x}' = \text{softsign}(\mathbf{W} \cdot \mathbf{x} + \mathbf{b}), \quad \text{softsign}(x) = \frac{x}{1 + |x|}, \quad (2)$$

where  $\mathbf{W}$  and  $\mathbf{b}$  are the learnable parameters inferred from the feedback collected in previous evaluations. The class of transformations described by Eq. 2 includes

slightly non-linear translations and rotations of the provided descriptors. While more complex transformations accounting for higher-order interactions between individual descriptors could potentially yield even more informative descriptors, a slightly non-linear transformation is inherently robust to overfitting,<sup>78</sup> and are more amenable to intuitive interpretation than more complex models.<sup>79</sup> We will demonstrate empirically in Secs. IV and V that this class of transformations is well suited for a variety of categorical optimization tasks.

Following a stochastic gradient optimization, the parameters  $\mathbf{W}$  and  $\mathbf{b}$  in Eq. 2 are adjusted to (i) increase the correlation between the newly generated descriptors  $\mathbf{x}'$  and the associated measurements, (ii) reduce correlations between newly generated descriptors, and (iii) remove redundant descriptors with poor correlations with the measurements or high correlations with other newly generated descriptors. These three goals are modeled as penalties which are to be minimized at training time (see supplementary information Sec. S.1.C for details).

## IV. SYNTHETIC BENCHMARKS

We empirically assess the performance of the introduced variants of GRYFFIN on a set of synthetic benchmark surfaces which are detailed in the supplementary information (see Sec. S.2). Four of the surfaces constitute categorized adaptations of established functions commonly used to benchmark global and local optimization strategies on continuous parameter domains. In addition, we include three partially and fully randomized surfaces with responses sampled from stationary probability distributions. While the ordering of the categorical options is arbitrary, we introduce a reference ordering to illustrate the surfaces (see supplementary information, Sec. S.2, for details). Unless noted otherwise, descriptors for the categorical options are generated such that they encode the reference ordering. Implementations of all benchmark surfaces are made available on GitHub.<sup>80</sup>

GRYFFIN is compared to a set of qualitatively different optimization strategies which are implemented in publicly available libraries: genetic optimization available through *PyEvolve*,<sup>48,49,81</sup> Bayesian optimization with random forests as implemented in *SMAC*,<sup>82–84</sup> Bayesian optimization with Gaussian processes via *GPyOpt*,<sup>70,85–87</sup> and Bayesian optimization with tree-structured Parzen windows introduced in *Hyperopt*.<sup>88,89</sup> In addition, we run random explorations of the candidate space as a baseline. We compare the performance of the different formulations of GRYFFIN to the other optimization strategies on all benchmark surfaces, probe the influence of the number of descriptors, study the scaling of GRYFFIN with the number of options per categorical variable and the number of categorical variables, and investigate the benefits of dynamic GRYFFIN over static GRYFFIN. For all comparisons, we measure the fraction of the candidate space that a given optimization strat-

egy explored to locate the best candidate. Unless noted otherwise, all comparisons are averaged over 200 independent executions of each strategy.

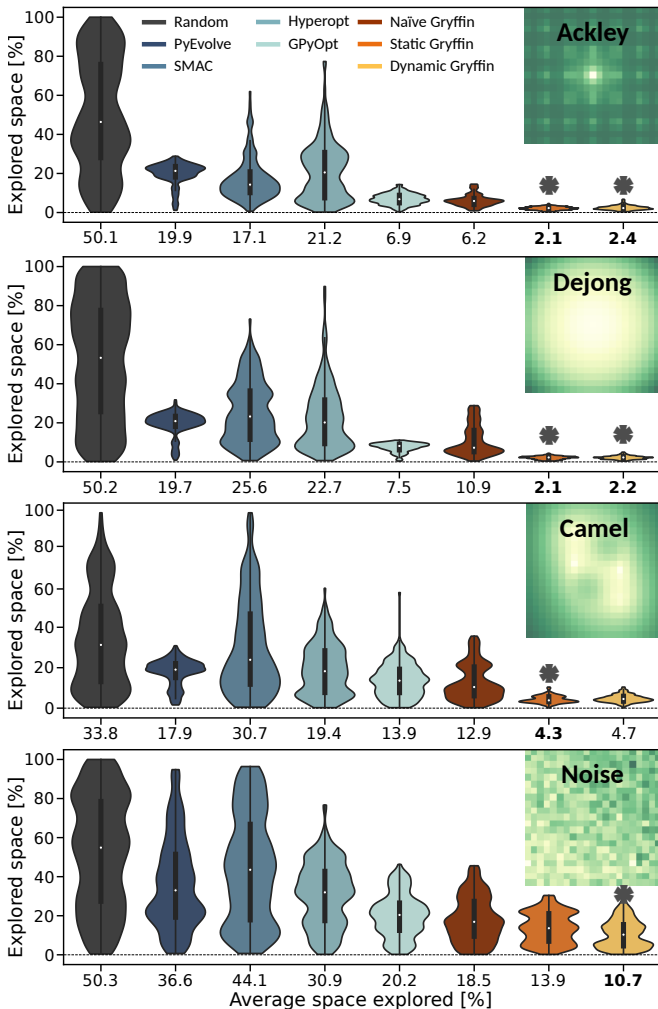


FIG. 2: Performance of various optimization strategies on selected synthetic surfaces. Individual panels indicate the fraction of the candidate space each algorithm explored before finding the global minimum of the surfaces illustrated on the top right (low values are shown in yellow, high values in green), averaged over 200 independent executions. Best performing algorithms are indicated in bold by a star. Color codes for the optimization strategies are shown in the top panel and apply to all panels in this figure.

### A. Optimization performance

In a first test, we compare the optimization strategies on two dimensional formulations of the synthetic benchmark surfaces with 21 options per dimension as illustrated in Fig. 2. The *Dejong* surface generalizes the convex parabola from continuous to categorical spaces, such that we consider it as *pseudo-convex*. In contrast, the *Ackley* surfaces is generalized from the Ackley path

function which is non-convex on the parameter domain. The *Camel* surface presents a degenerate global optimum as there are two different combinations of options which yield the same optimal response. Finally, the reference ordering of the *Noise* surface arranges the options such that they yield a relatively large local relative variance.<sup>†</sup> The fractions of the surfaces that the optimizers explored to locate their optima, averaged over 200 independent executions, are illustrated in Fig. 2. Full optimization traces are reported in the supplementary information (see Sec. S.3.B).

We observe, that a random exploration of the space requires the evaluation of approximately half the space for the surfaces with well-defined global optima, and about a third of the space for the *camel* function with a singly degenerate optimum. We find that the performances of *PyEvolve*, *SMAC* and *Hyperopt* are roughly comparable across the different surfaces, although *PyEvolve* tends to outperform *SMAC* and *Hyperopt* on the noiseless surfaces. *GPyOpt* generally locates global optima faster than the other strategies, but is slightly slower than naïve GRYFFIN on the non-convex surfaces. The faster optimization of convex surfaces with Gaussian process based Bayesian optimization compared to kernel density augmented Bayesian optimization has already been observed and discussed for continuous domains.<sup>68</sup> Notably, the static and dynamic formulations of GRYFFIN can significantly outperform the other optimization strategies, with reductions of the explored space by several factors. This observation confirms that providing real-valued descriptors can substantially accelerate the search. We also observe similar performances of the static and dynamic formulations of GRYFFIN for the deterministic surfaces (*Ackley*, *Dejong*, *Camel*), while dynamic GRYFFIN optimizes the noisy surface at a faster rate. This observation suggests that dynamic GRYFFIN is indeed capable of learning a more informative set of descriptors.

### B. Scaling to more options and higher dimensions

We further study the performance of GRYFFIN for larger candidate spaces with (i) more categorical variables, and (ii) more options per categorical variable. Increasing the number of variables or the number of options per variable generally increases the number of candidates in the space and is thus expected to require more candidate evaluations overall before the best candidate is identified. Results obtained for these benchmarks are detailed in the supplementary information (see Secs. S.3.C and S.3.D). The benchmarks suggest that GRYFFIN indeed uses more candidate evaluations to locate the global optimum with an increasing volume of the search space

<sup>†</sup>Note, that the locality of the variance in the response is measured with respect to the descriptor vectors of the associated options.

consistently across all benchmark surfaces. However, although the number of evaluations increases, the fraction of the explored space generally decreases. More specifically, we identify a polynomial decay of the explored space with an increasing number of options per variable, with decay exponents ranging from  $-1.0$  to  $-1.25$  and an exponential decay for an increase in the number of parameters with decay coefficients ranging from  $-1.6$  to  $-2.0$  across the different surfaces as shown in more detail in the supplementary information (see Secs. S.3.C and S.3.D). Based on this observation, we conclude that GRYFFIN may show an onset of the *curse of dimensionality*<sup>90</sup> only for a relatively large number of dimensions and indeed constitutes an optimization strategy which can navigate large categorical spaces efficiently.

### C. Data-driven refinement of descriptors

The effectiveness of transforming provided descriptors to accelerate the search for the best candidate is studied in detail on the *slope* surface with 51 options per dimension, resulting in 2,601 different candidates (see Fig. 3). For this benchmark, we randomly assign descriptors to each of the categorical options at a desired targeted correlation between the descriptors and the responses of the associated options. With a decreasing correlation, the local variance increases which results in a less structured space that is more challenging to navigate. We therefore generally expect a performance degradation for both static and dynamic GRYFFIN with decreasing correlation.

Fig. 3 illustrates the fractions of the candidate space explored by static and dynamic GRYFFIN for different targeted correlations between the supplied descriptors and the responses. For comparison, we also report the performance of the descriptor-less naïve formulation of GRYFFIN, which is independent of the supplied descriptors. We observe a significant increase in the fraction of the explored space with decreasing correlation for both static and dynamic GRYFFIN. Although both methods require more candidate evaluations with less informative descriptors, their performance never significantly degrades beyond the performance of the naïve formulation, indicating that even entirely uninformative descriptors do not delay the search for the best candidate compared to descriptor-less scenarios.

We further find that static GRYFFIN can benefit from descriptors and significantly outperform the naïve approach if the Pearson correlation coefficient between descriptors and responses is at least 0.8. Below this value, the average performance of static and naïve GRYFFIN is comparable, although the variance on the performance is higher for the static formulation. Similar to static GRYFFIN, learning a more informative set of descriptors with dynamic GRYFFIN accelerates the search more if the correlation between the descriptors and the responses is high. However, the dynamic formulation is generally at least as fast as the static formulation and can success-

fully leverage descriptors to outperform descriptor-less searches even at correlations as low as 0.1. We thus confirm that the descriptor transformation introduced in Eq. 2 is sufficiently robust to be applied to low-data tasks and conclude that deploying dynamic GRYFFIN can be beneficial for some descriptor guided optimization tasks without delaying the optimization compared to static GRYFFIN.

## V. APPLICABILITY OF GRYFFIN TO CHEMISTRY AND MATERIALS SCIENCE

Following the empirical benchmarks of GRYFFIN, we now demonstrate its applicability and practical relevance to a set of optimization tasks across materials science and chemistry. Specifically, we target the discovery of non-fullerene acceptors for organic solar cells, the design of organic-inorganic perovskites for light-harvesting and the selection of phosphine ligands simultaneously to the optimization of process conditions for Suzuki-Miyaura coupling reactions.

Obtaining statistically significant performance comparisons at a sufficient level of confidence requires the repeated execution of optimization runs to average out the influences of initial conditions and probabilistic elements of the optimization strategies. As repetitive executions of optimization runs on these applications are highly resource demanding, we construct these optimization tasks from recently reported datasets: the applications on the discovery of non-fullerene acceptors and perovskites are based on lookup tables, and the optimization of Suzuki reactions are facilitated via a probabilistic model trained on experimental data (*virtual robot*) to emulate experimental uncertainties in addition to the average response. Virtual robots have recently been introduced to benchmark algorithms for autonomous experimentation in the context of multi-objective optimization.<sup>91</sup>

The selection of physicochemical descriptors for the categorical variables of these three applications is mostly motivated by their accessibility. Determining the most suitable set of descriptors for a given application requires repeated measurements of the property of interest, which typically is a highly resource demanding process. As such, the selection of the descriptors as outlined in the following sections balances applicability and availability, as the most informative set of descriptors for a scientific discovery task might be *a priori* unknown. The physicochemical descriptors used in the following three applications are available on GitHub.<sup>80</sup>

### A. Discovery of non-fullerene acceptor candidates for organic photovoltaics

Small organic molecules currently constitute the highest performing acceptor materials for organic solar cells.<sup>92,93</sup> The large number of degrees of freedom when

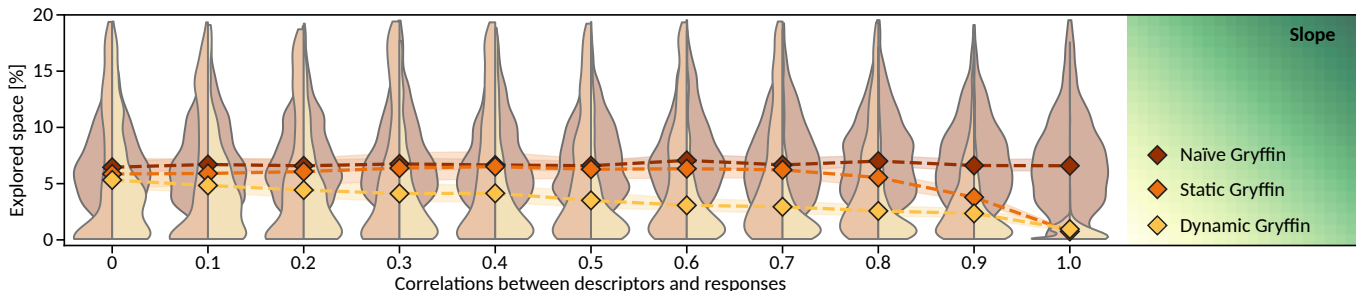


FIG. 3: Behavior of naïve, static and dynamic GRYFFIN on the slope surface for different descriptors. Descriptors have been generated randomly with a targeted correlation between the descriptors and the response of the associated options.

designing such non-fullerene acceptors, arising from complex aromatic molecular geometries, allows to fine tune their relevant electronic properties, for example the optical gap and the energy level alignment between the donor and acceptor materials. Despite their flexibility, the large design space for non-fullerene acceptors poses major obstacles to the discovery of promising candidate molecules.

We demonstrate the applicability of GRYFFIN for the discovery of non-fullerene acceptors on a candidate space of 4,216 different small organic molecules, which form a subset of a recently reported comprehensive study.<sup>94</sup> Acceptor candidates in this library are constructed from a set of molecular fragments which are separated into three fragment pools (see Fig. 4a). Each candidate is composed of one core fragment  $C$  (8 options), two spacer fragments  $S$  (31 options), and two terminal fragments  $T$  (17 options) following a symmetric design. Details on the library of candidate fragments are reported in the supplementary information (see Sec. S.4.A). The performance of each acceptor candidate is quantified based on the power conversion efficiency (PCE) which is computed following a workflow based on the data-driven calibration of DFT results.<sup>94</sup> The optimization task targets the maximization of the expected PCE of the acceptor candidate.

We guide static and dynamic GRYFFIN with a set of electronic and geometric descriptors for each of the fragments: the HOMO and LUMO energy levels, the dipole moment, the radius of gyration and the molecular weight. Electronic properties were computed at the B3LYP/Def2SVP level of theory on a SuperFineGrid using Gaussian,<sup>95</sup> and the radius of gyration was computed for the ground state conformations of the molecules. The correlations of the descriptors with the PCE of the resulting non-fullerene acceptor are generally low, with the highest encountered Pearson correlation coefficients reaching values of about 0.2 (see supplementary information, Sec. S.4.A, for details). In fact, the identification of improved descriptors for the accurate prediction of PCE in organic solar cells is an active field of research.<sup>96–98</sup>

Fig. 4b illustrates the fraction of the candidate library (averaged over 200 independent executions) which each optimization strategy explored before identifying the combination of fragments which yields the highest PCE. Full optimization traces for each of the optimiza-

tion strategies are reported in the supplementary information (see Sec. S.4.A). In agreement with the synthetic tests (see Sec. IV), we find that *PyEvolve* explores smaller fractions (21 %) of the space than *Hyperopt* (27 %) or *SMAC* (41 %). The performance of naïve GRYFFIN, exploring about 11 %, is comparable to *GPyOpt* and thus significantly faster than the other benchmark strategies. However, the physical descriptors supplied for each of the fragments enable static GRYFFIN to find the best acceptor candidate after exploring only 8.7 % of the candidate space ( $\sim 22\%$  reduction of the required acceptor evaluations) while dynamic GRYFFIN can refine the supplied descriptors to find the best candidate with only 6.9 % of the library explored ( $\sim 38\%$  reduction over naïve search). This improvement of dynamic GRYFFIN over static GRYFFIN confirms that the supplied descriptors can be transformed into a more informative set to accelerate the search.

Fig. 4c illustrates the importance of individual descriptors to guide the search, as determined by *dynamic* GRYFFIN. Specifically, we plot the relative contributions of individual descriptors to the set of the transformed descriptors which were used when the best performing candidate was identified. We observe that the descriptor search emphasizes the relevance of electronic descriptors over geometric descriptors consistently across all types of fragments. Indeed, the Scharber model is designed to estimate PCEs qualitatively from the electronic properties of the acceptor material,<sup>99,100</sup> and further refinements can be enabled by considering the bandgap. The design of non-fullerene acceptor candidates beyond the provided library could therefore be inspired mostly by the electronic properties of the fragments rather than their geometric properties, although even more informative descriptors could potentially be constructed with more computational effort.<sup>96</sup>

## B. Discovery of hybrid organic-inorganic perovskites for light-harvesting

Perovskite solar cells constitute another class of light-harvesting materials which are typically composed of inorganic lead halide matrices and contain inorganic or or-

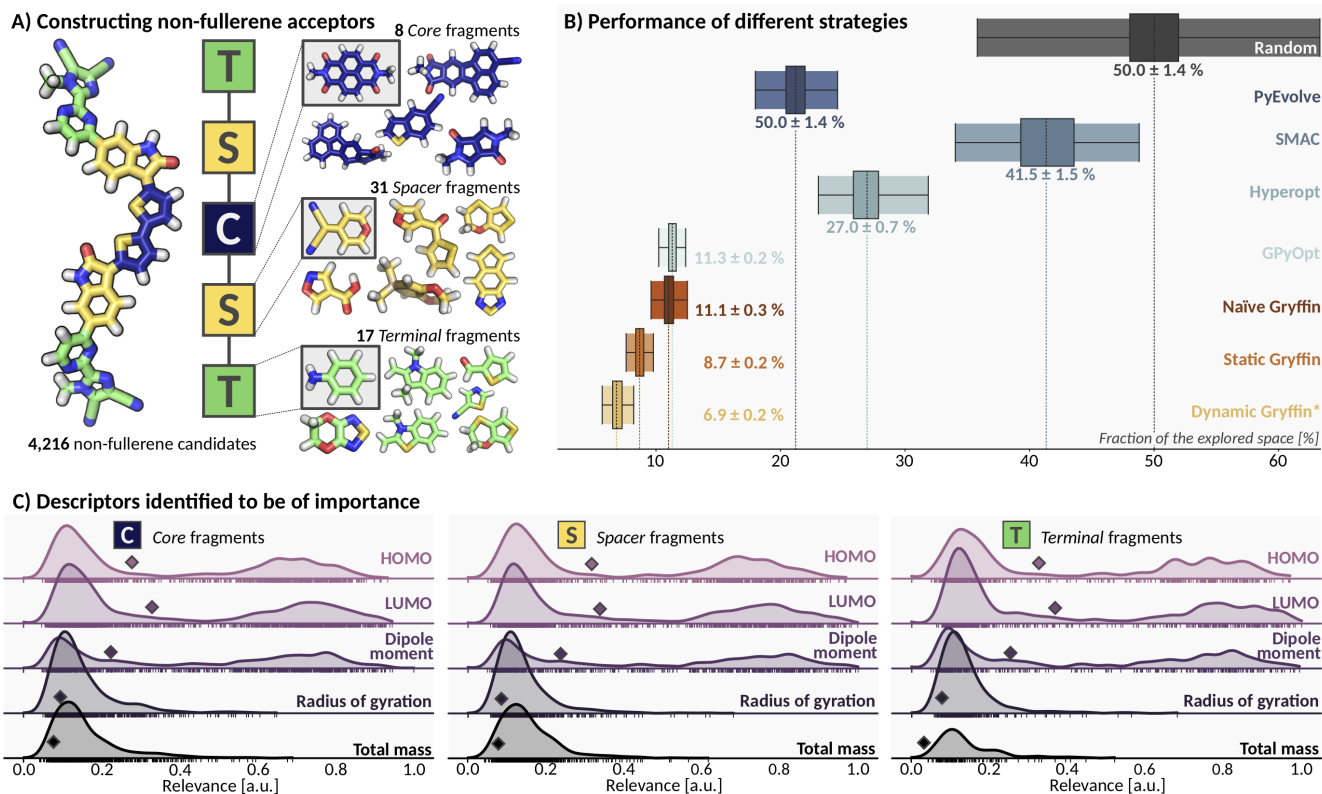


FIG. 4: Performance of GRYFFIN on the task of identifying non-fullerene acceptors for maximized power conversion efficiencies. (A) Non-fullerene acceptor candidates are constructed from a set of molecular fragments (core, spacer and terminal) which are symmetrically arranged to span a library of 4,216 different candidate molecules. (B) Fraction of the candidate library to be explored by each of the studied optimization strategies to identify the best performing acceptor candidate. (C) Most informative descriptors to guide the search of *dynamic* GRYFFIN. Diamonds indicate the average relevance of each descriptor.

ganic anions (see Fig. 5a).<sup>101–103</sup> Recently, perovskite solar cells have experienced increased attention as breakthroughs in materials and device architectures boosted their efficiencies and stabilities.<sup>104</sup> Yet, the discovery of a viable perovskite designs involves numerous choices regarding material compositions and process parameters, which poses a challenge to the rapid advancement of this light-harvesting technology. This second demonstration of the applicability of GRYFFIN focuses on the discovery of hybrid organic-inorganic perovskites (HOIPs) based on a recently reported dataset.<sup>105</sup> The HOIP candidates of this dataset are designed from a set of four different halide anions, three different group-IV cations and 16 different organic anions, resulting in 192 different HOIP compositions. Among other properties, the datasets reports the bandgaps of the HOIP candidates obtained from DFT calculations with GGA and the HSE06 functional. In this application, we aim to minimize the bandgap.

The inorganic constituents are characterized by their electron affinity, ionization energy, mass and electronegativity to guide the searches of the static and dynamic formulations of GRYFFIN. The organic compounds are described by their HOMO and LUMO energy levels, dipole moment, atomization energy, radius of gyration and

molecular weight. All electronic descriptors were computed at the HSEH1PBE/Def2QZVPP level of theory on a SuperFineGrid with Gaussian,<sup>95</sup> and the radii of gyration are calculated for the ground state conformer. Note, that in contrast to the search for viable non-fullerene acceptors, this application presents an optimization task which not only features physically different descriptors between individual categorical variables, but also varying dimensionalities of the descriptors associated with individual categorical variables. However, the correlations between individual descriptors and the expected bandgaps of the assembled HOIP materials are significantly higher compared to the descriptors used for the non-fullerene acceptors (see supplementary information, Sec. S.4.B, for additional details).

The fractions of the candidate space explored by each optimization strategy before locating the HOIP composition with the lowest bandgap are illustrated in Fig. 5b. More detailed results are reported in the supplementary information (see Sec. S.4.B). Similarly to the synthetic benchmarks (see Sec. IV) and the optimization of non-fullerene acceptors (see Sec. V.A), we find that all optimization strategies outperform a purely random exploration of the candidate space. Bayesian optimization strategies tend to locate the best performing HOIP candi-



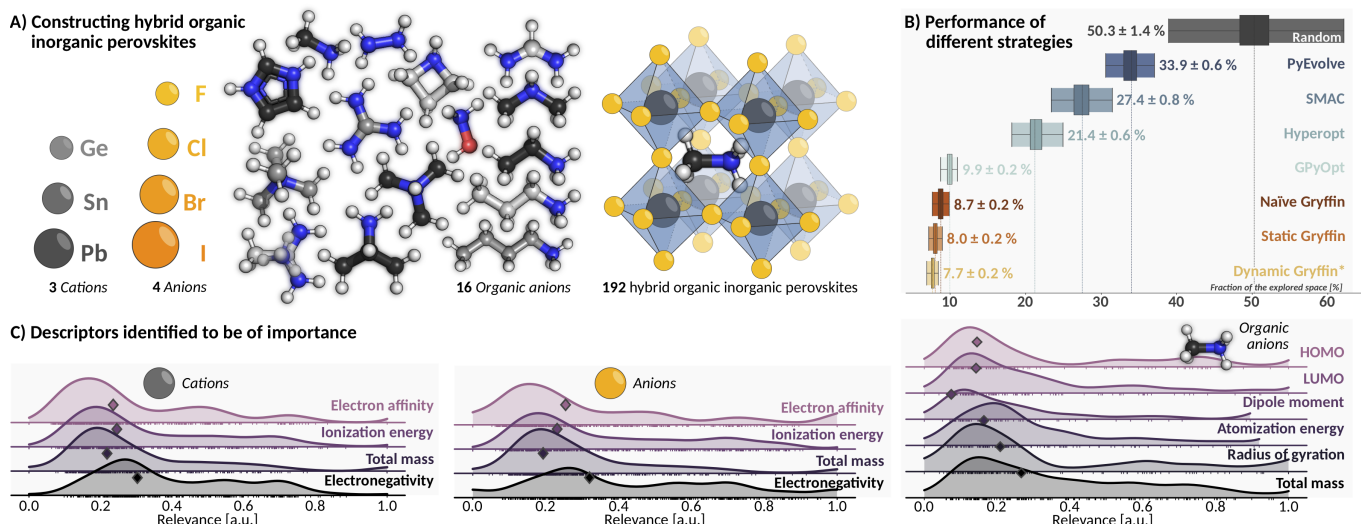


FIG. 5: Results of the benchmarks on hybrid organic inorganic perovskites. (A) Perovskites are assembled by choosing one of three inorganic cations, one of four inorganic anions and one of 16 organic anions, resulting in 192 unique designs. (B) Fractions of the candidate library to be explored by each of the studied optimization strategies to identify the perovskite design with the lowest bandgap. (C) Most informative descriptors to guide the optimization for each of the three constituents identified by dynamic GRYFFIN. Diamonds indicate the average relevance of each descriptor.

date at a faster rate than *PyEvolve* ( $\sim 34\%$ ), with *GPyOpt* evaluating only about 10% of the candidate space, followed by *Hyperopt* ( $\sim 21\%$ ) and *SMAC* ( $\sim 27\%$ ). Yet, naïve GRYFFIN succeeds after exploring less than 9% of the search space. Note, that this fraction of the search space corresponds to roughly 17 HOIP candidates which approximately matches the number of available organic compounds.

The static and dynamic formulations of GRYFFIN even undercut this value and identify the best performing HOIP within less than 8%, corresponding to the evaluation of less than 16 HOIP candidates on average. This observation confirms that GRYFFIN indeed accelerates the optimization of categorical variables if physical descriptors are available. However, we no longer observe a significant performance difference between the static and the dynamic formulation of GRYFFIN, which is in agreement with the significantly higher correlation between provided descriptors and the bandgaps and the observations made on the synthetic surfaces (see Sec. IV.C). For this application, we find that electronegativity is most relevant for the inorganic constituents, while the radius of gyration and the molecular weight are most informative for the organic compound. Although the targeted property (bandgap of the HOIP) is an electronic property, dynamic GRYFFIN seems to benefit the most from the geometric (and not the electronic) descriptors of the organic compound. In contrast, the mass of the inorganic compounds seems to be the least relevant, while their electronegativity is most informative. These observations suggest that the organic molecule does not directly affect the electronic properties of the HOIP material, but rather induces a change in the arrangement of the inorganic compounds which in turn modulates the bandgap.

Indeed, this hypothesis has emerged in various studies on perovskite materials,<sup>106–110</sup> which confirms that dynamic GRYFFIN can capture the relevant trends in the descriptors and inspire future design choices.

### C. Suzuki-Miyaura cross-coupling optimization

As a final application, we demonstrate how GRYFFIN can aid in the optimization of Suzuki-Miyaura cross-coupling reactions with heterocyclic substrates.<sup>111</sup> These reactions are of particular interest to the pharmaceutical industry,<sup>112</sup> and have recently been studied in the context of self-optimizing reactors for flow chemistry.<sup>36–38</sup> The optimization of chemical reactions typically targets a maximization of the yield. The yield of a reaction can be modified by varying a set of process conditions which can largely be described by continuous variables. However, the yield can also be increased by using suitable catalytic systems which modulate the rate of the reaction.

For the example of a flow-based Suzuki-Miyaura cross-coupling reaction, we specifically consider three continuous reaction conditions (temperature, residence time, catalyst loading) and one categorical variable (ligand for Palladium catalyst) as illustrated in Fig. 6a. The optimization task targets the maximization of the reaction yield, while simultaneously maximizing the turnover number (TON) of the catalyst. We employ the *Chimera* scalarizing strategy<sup>91</sup> to enable this multi-objective optimization, where we accept a 10% degradation on the maximum achievable reaction yield to increase the TON as the secondary objective. This acceptable degradation

corresponds to a desired reaction yield of above 85.4%. GRYFFIN is integrated with the PHOENICS algorithm to simultaneously optimize categorical and continuous parameters. We consider a set of seven ligands (see Fig. 6b) which are characterized by their molecular weight, the number of rotatable bonds, their melting points, the number of valence electrons and their partition coefficients, quantified by  $\log P$ . Details on the physicochemical descriptors and the ranges for the continuous parameters are provided in the supplementary information (see Sec. S.4.C).

As a complete performance analysis of the different optimization strategies is experimentally not tractable, we emulate noisy experimental responses with a probabilistic model which is trained on experimental data, as previously demonstrated for benchmarking multi-objective optimization strategies.<sup>91</sup> Specifically, we train a Bayesian neural network to reproduce the reaction yield and TON of a previously reported flow-based reactor.<sup>37</sup> Details on the data acquisition, model training and prediction accuracies are provided in the supplementary information (see Sec. S.4.C). The coefficients of determination of the trained model for the test set predictions of the reaction yield and the TON are above  $r^2 > 0.96$  which indicates that the trained model indeed constitutes a realistic approximation to the experimental surface. With this experimental emulator, we execute 200 independent optimization runs with 240 evaluations for each of the benchmarked experiment planning strategies.

Fig. 6c illustrates the performance of the individual optimization strategies. We find, that *GPyOpt* requires about 18 evaluations to identify reaction conditions which achieve desired reaction yields of above 85.4%. The other benchmark strategies, including random exploration, satisfy this first objective already after evaluating approximately 10-12 different conditions. Only the three formulations of GRYFFIN can locate desired reaction conditions at an even faster rate, requiring 7-8 evaluations. For the subsequent maximization of the TON we observe that *PyEvolve* is the slowest of the optimization strategy. In fact, the random search strategy outperforms *PyEvolve* after about 100 evaluations. Despite its relatively poor performance for the reaction yield, *GPyOpt* maximizes the TON faster than random search. Yet, *SMAC* and *Hyperopt* still achieve significantly higher TONs for any given number of evaluations and are slightly outperformed by GRYFFIN. We do not observe a significant difference in the performance of the three formulations of GRYFFIN which can be attributed to the fact that we only have one categorical variable with only seven options to choose from. Nevertheless, we observe a slight trend that dynamic GRYFFIN achieves a little higher TONs than static or naïve GRYFFIN.

The contributions of individual descriptors are illustrated in Fig. 6d, where we find that the number of valence electrons shows the highest relevance among all descriptors to guide dynamic GRYFFIN, while the number of rotatable bonds is the least relevant. Indeed, the number

of rotatable bonds correlates the least with the maximum and average reaction yields and TONs for any values of the other parameters (see supplementary information, Sec. S.4.C), confirming that dynamic GRYFFIN correctly identifies non-informative descriptors within the given library of ligand candidates. The number of valence electrons also correlates strongly with the maximum achievable reaction yield for each of the ligands, confirming that this descriptor is highly informative to identify ligands which satisfy the reaction yield threshold. Melting point and molecular weight are likely indicated as relevant due to their strong correlation with the number of valence electrons. Based on the indications of dynamic GRYFFIN, the design of more potent ligand candidates could be inspired by the number of valence electrons. However, it is important to mention that here, in contrast to the other applications, we considered a relatively small library of only seven ligands, such that the descriptor indications might not necessarily generalize well to larger libraries.

Overall, across all three applications, we find that naïve GRYFFIN generally constitutes a competitive strategy for the optimization of categorical variables in chemistry and materials science which tends to outperform state-of-the-art optimization strategies without leveraging physicochemical descriptors in the selection process. Static GRYFFIN can accelerate the search with provided descriptors and navigate the search space more efficiently by exploiting descriptor-based similarities between individual options, thus efficiently leveraging domain knowledge. Dynamic GRYFFIN can accelerate the search even further by transforming provided descriptors to improve their relevance and inspire scientific insights. Finally, GRYFFIN integrates well with optimization strategies for continuous variables and thus enables the simultaneous optimization of mixed continuous-categorical parameter spaces.

## VI. CONCLUSION

In this work we introduced GRYFFIN, an experiment planning strategy for the selection of categorical variables such as functional molecules, catalysts or material constituents in autonomous experimentation workflows. GRYFFIN can leverage domain knowledge in the form of physicochemical descriptors for each of the categorical options, and inspire design choices and scientific insights while efficiently navigating the search space. To this end, GRYFFIN is based on the idea to augment Bayesian optimization with Bayesian kernel density estimation, which has recently been introduced for continuous optimization domains.<sup>68</sup> Using smooth approximations to categorical distributions and locally transforming the metric of the optimization domain, GRYFFIN is able to exploit similarity information between categorical options to accelerate the search for promising molecules and materials.

We assessed the performance of GRYFFIN in compari-



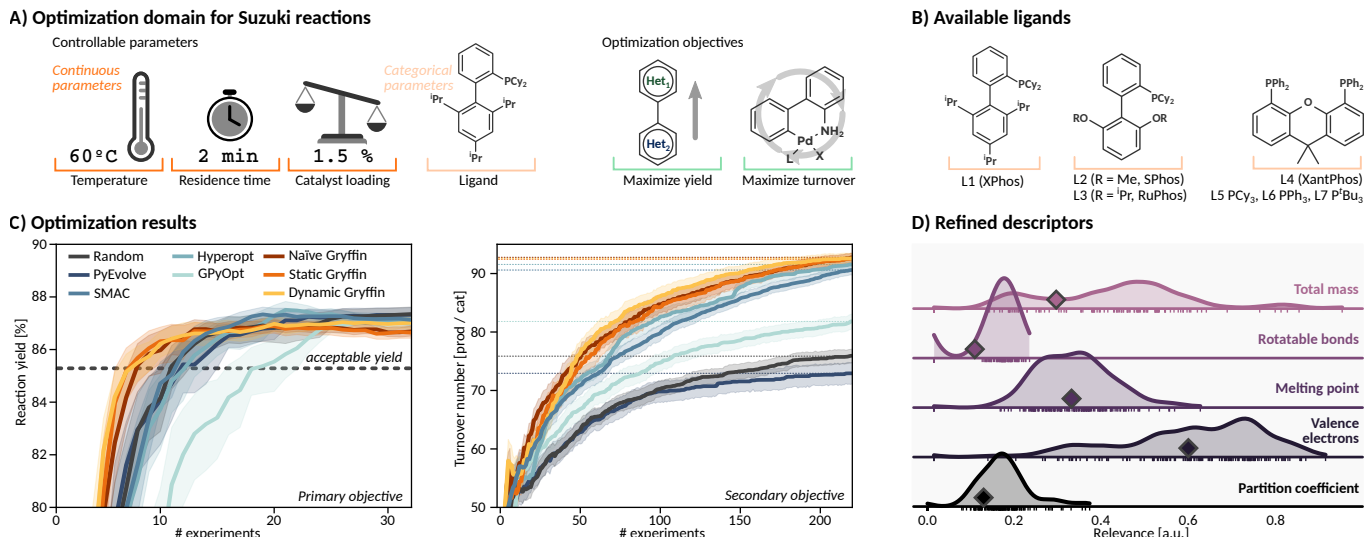


FIG. 6: Results of the benchmarks on the optimization of Suzuki-Miyaura reactions. (A) Parameters and objectives for the optimization task: We target the identification of optimal values for three process parameters (temperature, residence time, catalyst loading) and one categorical variable (ligand) to maximize the yield of the reaction and the turnover number (TON) of the catalyst. (B) Illustration of the seven available ligands. (C) Optimization traces showing the performance of individual optimization strategies. (D) Most informative descriptors to guide the optimization. Diamonds indicate the average relevance of each descriptor.

son to state-of-the-art strategies to select categorical variables on a set of synthetic benchmark functions. Our benchmarks indicate that the naïve formulation of GRYFFIN, which does not use any descriptor information, is competitive on *pseudo* convex surfaces and outperforms the other strategies on all other surfaces. Descriptor-guided searches with static GRYFFIN identify global optima at significantly faster rates consistently for all surfaces. Dynamic GRYFFIN, which attempts to construct a more informative set of descriptors, can accelerate the search even further in some cases, especially for moderate correlations between the descriptors and the responses and noisy environments.

The capabilities of GRYFFIN were further demonstrated on three real-world applications across materials science and chemistry: (i) the discovery of non-fullerene acceptors for organic solar cells, (ii) the discovery of hybrid organic-inorganic perovskites for light-harvesting, and (iii) the mixed categorical-continuous selection of ligands and reaction conditions for Suzuki-Miyaura cross-coupling reactions. GRYFFIN outperforms the other experiment planning strategies in all three applications. Static and dynamic GRYFFIN can accelerate the searches even with moderately informative physicochemical descriptors. We further find that dynamic GRYFFIN can identify trends among the descriptors which elucidate some of the prevalent phenomena which give rise to the properties of interest, indicating that dynamic GRYFFIN has the potential to foster scientific understanding and encourage physical and chemical intuition for the studied systems.

Based on the synthetic and real-world benchmarks, we suggest that GRYFFIN constitutes a readily available

strategy for the efficient selection of categorical variables in data-driven experimentation workflows and alleviates some of the immediate challenges to the versatile deployment of autonomous experimentation platforms. The demonstrated acceleration of the search based on physicochemical descriptors constitutes a step towards autonomous experimentation guided by domain knowledge. In summary, we believe that GRYFFIN has the potential to accelerate scientific discovery and invite the community to test and deploy it to scenarios where evaluations of categorical parameters are expensive and similarities between categorical options can be defined. GRYFFIN is available for download on GitHub.<sup>80</sup>

## Acknowledgments

The authors thank Dr. Matteo Aldeghi, Melodie Christensen, Dr. Pascal Friederich, Dr. Gabriel dos Passos Gomes and Dr. Daniel P. Tabor for valuable and insightful discussions. F.H. acknowledges financial support from the Herchel Smith Graduate Fellowship and the Jacques-Emile Dubois Student Dissertation Fellowship. L.M.R and A.A.G were supported by the Tata Sons Limited - Alliance Agreement (A32391). A.A.G. would like to thank Dr. Anders Frøseth for his support. This work relates to Department of Navy award (N00014-19-1-2134) issued by the Office of Naval Research. The United States Government has a royalty-free license throughout the world in all copyrightable material contained herein. Any opinions, findings, and conclusions or recommendations expressed in this material are those of the authors and do not necessarily reflect the views of the Office of Naval Research.

All computations reported in this paper were completed on the Arran cluster supported by the Health Sciences Platform (HSP) at Tianjin University, P.R. China and

the Odyssey cluster supported by the FAS Division of Science, Research Computing Group at Harvard University.

- [1] Daniel P Tabor, Loïc M Roch, Semion K Saikin, Christoph Kreisbeck, Dennis Sheberla, Joseph H Montoya, Shyam Dwaraknath, Muratahan Aykol, Carlos Ortiz, Hermann Tribukait, et al. Accelerating the discovery of materials for clean energy in the era of smart automation. *Nat. Rev. Mater.*, 3:5–20, 2018.
- [2] Juan-Pablo Correa-Baena, Kedar Hippalgaonkar, Jeroen van Duren, Shaffiq Jaffer, Vijay R Chandrasekhar, Vladan Stevanovic, Cyrus Wadia, Supratik Guha, and Tonio Buonassisi. Accelerating materials development via automation, machine learning, and high-performance computing. *Joule*, 2(8):1410–1420, 2018.
- [3] Selim M Senkan. High-throughput screening of solid-state catalyst libraries. *Nature*, 394(6691):350, 1998.
- [4] Wilhelm F Maier, Klaus Stoewe, and Simone Sieg. Combinatorial and high-throughput materials science. *Angewandte chemie international edition*, 46(32):6016–6067, 2007.
- [5] Hideomi Koinuma and Ichiro Takeuchi. Combinatorial solid-state chemistry of inorganic materials. *Nature materials*, 3(7):429, 2004.
- [6] Ricardo Macarron, Martyn N Banks, Dejan Bojanic, David J Burns, Dragan A Cirovic, Tina Garyantes, Darren VS Green, Robert P Hertzberg, William P Janzen, Jeff W Paslay, et al. Impact of high-throughput screening in biomedical research. *Nature reviews Drug discovery*, 10(3):188, 2011.
- [7] Steven M Mennen, Carolina Alhambra, C Liana Allen, Mario Barberis, Simon Berritt, Thomas A Brandt, Andrew D Campbell, Jesús Castañón, Alan H Cherney, Melodie Christensen, et al. The evolution of high-throughput experimentation in pharmaceutical development and perspectives on the future. *Organic Process Research & Development*, 23(6):1213–1242, 2019.
- [8] Konstantin Troshin and John F Hartwig. Snap deconvolution: An informatics approach to high-throughput discovery of catalytic reactions. *Science*, 357(6347):175–181, 2017.
- [9] Joshua A Selekman, Jun Qiu, Kristy Tran, Jason Stevens, Victor Rosso, Eric Simmons, Yi Xiao, and Jacob Janey. High-throughput automation in chemical process development. *Annual review of chemical and biomolecular engineering*, 8:525–547, 2017.
- [10] Lei Cheng, Rajeev S Assary, Xiaohui Qu, Anubhav Jain, Shyue Ping Ong, Nav Nidhi Rajput, Kristin Persson, and Larry A Curtiss. Accelerating electrolyte discovery for energy storage with high-throughput screening. *The journal of physical chemistry letters*, 6(2):283–291, 2015.
- [11] Karl D Collins, Tobias Gensch, and Frank Glorius. Contemporary screening approaches to reaction discovery and development. *Nature chemistry*, 6(10):859, 2014.
- [12] Andrew McNally, Christopher K Prier, and David WC MacMillan. Discovery of an  $\alpha$ -amino c-h arylation reaction using the strategy of accelerated serendipity. *Science*, 334(6059):1114–1117, 2011.
- [13] Katharine W Moore, Alexander Pechen, Xiao-Jiang Feng, Jason Dominy, Vincent J Beltrani, and Herschel Rabitz. Why is chemical synthesis and property optimization easier than expected? *Physical Chemistry Chemical Physics*, 13(21):10048–10070, 2011.
- [14] Florian Häse, Loïc M Roch, and Alán Aspuru-Guzik. Next-generation experimentation with self-driving laboratories. *Trends in Chemistry*, 10.1016/j.trechm.2019.02.007, 2019.
- [15] Klavs F Jensen, Connor W Coley, and Natalie S Eyke. Autonomous discovery in the chemical sciences part i: Progress. *Angewandte Chemie International Edition*, 2019.
- [16] Connor W Coley, Natalie S Eyke, and Klavs F Jensen. Autonomous discovery in the chemical sciences part ii: Outlook. *Angewandte Chemie International Edition*, 2019.
- [17] Loïc M Roch, Florian Häse, Christoph Kreisbeck, Teresa Tamayo-Mendoza, Lars PE Yunker, Jason E Hein, and Alán Aspuru-Guzik. Chemos: Orchestrating autonomous experimentation. *Science Robotics*, 3(19):eaat5559, 2018.
- [18] Mari Yoshida, Trevor Hinkley, Soichiro Tsuda, Yousef M Abul-Haija, Roy T McBurney, Vladislav Kulikov, Jennifer S Mathieson, Sabrina Galiñanes Reyes, Maria D Castro, and Leroy Cronin. Using evolutionary algorithms and machine learning to explore sequence space for the discovery of antimicrobial peptides. *Chem*, 4(3):533–543, 2018.
- [19] Connor W Coley, Dale A Thomas, Justin AM Lummiss, Jonathan N Jaworski, Christopher P Breen, Victor Schultz, Travis Hart, Joshua S Fishman, Luke Rogers, Hanyu Gao, et al. A robotic platform for flow synthesis of organic compounds informed by ai planning. *Science*, 365(6453):eaax1566, 2019.
- [20] Zhenpeng Zhou, Xiaocheng Li, and Richard N Zare. Optimizing chemical reactions with deep reinforcement learning. *ACS central science*, 3(12):1337–1344, 2017.
- [21] Vasilios Duros, Jonathan Grizou, Weimin Xuan, Zied Hosni, De-Liang Long, Haralampos N Miras, and Leroy Cronin. Human versus robots in the discovery and crystallization of gigantic polyoxometalates. *Angewandte Chemie*, 129(36):10955–10960, 2017.
- [22] Fang Ren, Logan Ward, Travis Williams, Kevin J Laws, Christopher Wolverton, Jason Hattrick-Simpers, and Apurva Mehta. Accelerated discovery of metallic glasses through iteration of machine learning and high-throughput experiments. *Science advances*, 4(4):eaag1566, 2018.
- [23] Michael J Casciato, Sungil Kim, JC Lu, Dennis W Hess, and Martha A Grover. Optimization of a carbon dioxide-assisted nanoparticle deposition process using sequential experimental design with adaptive design space. *Industrial & Engineering Chemistry Research*, 51(11):4363–4370, 2012.
- [24] Paul B Wigley, Patrick J Everitt, Anton van den Hengel, JW Bastian, Mahasen A Sooriyabandara, Gordon D McDonald, Kyle S Hardman, CD Quinlivan, P Manju,

- Carlos CN Kuhn, et al. Fast machine-learning online optimization of ultra-cold-atom experiments. *Scientific reports*, 6:25890, 2016.
- [25] Helge S Stein and John M Gregoire. Progress and prospects for accelerating materials science with automated and autonomous workflows. *Chemical Science*, 10(42):9640–9649, 2019.
- [26] Anne-Catherine Bédard, Andrea Adamo, Kosi C Aroh, M Grace Russell, Aaron A Bedermann, Jeremy Torosian, Brian Yue, Klavs F Jensen, and Timothy F Jamison. Reconfigurable system for automated optimization of diverse chemical reactions. *Science*, 361(6408):1220–1225, 2018.
- [27] Daniel Cortés-Borda, Eric Wimmer, Boris Gouilleux, Elvina Barré, Nicolas Oger, Lubna Goulamaly, Louis Peault, Benoît Charrier, Charlotte Truchet, Patrick Girardeau, et al. An autonomous self-optimizing flow reactor for the synthesis of natural product carpanone. *The Journal of organic chemistry*, 83(23):14286–14299, 2018.
- [28] Daniel E Fitzpatrick, Claudio Battilocchio, and Steven V Ley. A novel internet-based reaction monitoring, control and autonomous self-optimization platform for chemical synthesis. *Organic Process Research & Development*, 20(2):386–394, 2015.
- [29] Pavel Nikolaev, Daylond Hooper, Frederick Webber, Rahul Rao, Kevin Decker, Michael Krein, Jason Poleski, Rick Barto, and Benji Maruyama. Autonomy in materials research: a case study in carbon nanotube growth. *npj Computational Materials*, 2:16031, 2016.
- [30] Benji Maruyama, Kevin Decker, Pavel Nikolaev, Michael Krein, Jason Poleski, and Rick Barto. Autonomous experimentation applied to carbon nanotube synthesis. In *Meeting Abstracts*, number 9, pages 668–668. The Electrochemical Society, 2017.
- [31] Marcus M Noack, Kevin G Yager, Masafumi Fukuto, Gregory S Doerk, Ruipeng Li, and James A Sethian. A kriging-based approach to autonomous experimentation with applications to x-ray scattering. *Scientific reports*, 9(1):1–19, 2019.
- [32] Aaron Gilad Kusne, Tieren Gao, Apurva Mehta, Liqin Ke, Manh Cuong Nguyen, Kai-Ming Ho, Vladimir Antropov, Cai-Zhuang Wang, Matthew J Kramer, Christian Long, et al. On-the-fly machine-learning for high-throughput experiments: search for rare-earth-free permanent magnets. *Scientific reports*, 4:6367, 2014.
- [33] Benjamin P MacLeod, Fraser GL Parlane, Thomas D Morrissey, Florian Häse, Loïc M Roch, Kevan E Detelbach, Raphaell Moreira, Lars PE Yunker, Michael B Rooney, Joseph R Deeth, et al. Self-driving laboratory for accelerated discovery of thin-film materials. *arXiv preprint arXiv:1906.05398*, 2019.
- [34] Jiagen Li, Yuxiao Tu, Rulin Liu, Yihua Lu, and Xi Zhu. Toward on-demand materials synthesis and scientific discovery through intelligent robots. *Advanced Science*, page 1901957, 2020.
- [35] Stefan Langner, Florian Häse, José Darío Perea, Tobias Stubhan, Jens Hauch, Loïc M Roch, Thomas Heumueller, Alán Aspuru-Guzik, and Christoph J Brabec. Beyond ternary opv: High-throughput experimentation and self-driving laboratories optimize multi-component systems. *Adv. Mater.*, 2020.
- [36] Lorenz M Baumgartner, Connor W Coley, Brandon J Reizman, Kevin W Gao, and Klavs F Jensen. Optimum catalyst selection over continuous and discrete process variables with a single droplet microfluidic reaction platform. *Reaction Chemistry & Engineering*, 3(3):301–311, 2018.
- [37] Brandon J Reizman, Yi-Ming Wang, Stephen L Buchwald, and Klavs F Jensen. Suzuki–miyaura cross-coupling optimization enabled by automated feedback. *Reaction chemistry & engineering*, 1(6):658–666, 2016.
- [38] Brandon J Reizman and Klavs F Jensen. Simultaneous solvent screening and reaction optimization in microliter slugs. *Chemical Communications*, 51(68):13290–13293, 2015.
- [39] Jasper Snoek, Hugo Larochelle, and Ryan P Adams. Practical bayesian optimization of machine learning algorithms. In *Advances in neural information processing systems*, pages 2951–2959, 2012.
- [40] Daniel J Lizotte, Tao Wang, Michael H Bowling, and Dale Schuurmans. Automatic gait optimization with gaussian process regression. In *IJCAI*, volume 7, pages 944–949, 2007.
- [41] Yang Bai, Liam Wilbraham, Benjamin J Slater, Martijn A Zwijnenburg, Reiner Sebastian Sprick, and Andrew I Cooper. Accelerated discovery of organic polymer photocatalysts for hydrogen evolution from water through the integration of experiment and theory. *Journal of the American Chemical Society*, 141(22):9063–9071, 2019.
- [42] J. S. Bergstra and Y. Bengio. Random search for hyperparameter optimization. *Journal of Machine Learning Research*, 13(Feb):281–305, 2012.
- [43] N Baba. Convergence of a random optimization method for constrained optimization problems. *Journal of Optimization Theory and Applications*, 33(4):451–461, 1981.
- [44] J Matyas. Random optimization. *Automation and Remote control*, 26(2):246–253, 1965.
- [45] M. J. Anderson and P. J. Whitcomb. *DOE simplified: practical tools for effective experimentation*. CRC Press, 2016.
- [46] G. E. P. Box, J. S. Hunter, and W. G. Hunter. *Statistics for experimenters: design, innovation and discovery*, volume 2. 2005.
- [47] R. A. Fisher. *The design of experiments*. Oliver and Boyd; Edinburgh; London, 1937.
- [48] J. H. Holland and D. Goldberg. Genetic algorithms in search, optimization and machine learning. *Massachusetts: Addison-Wesley*, 1989.
- [49] R John. Genetic programming: on the programming of computers by means of natural selection, 1992.
- [50] Mandavilli Srinivas and Lalit M Patnaik. Genetic algorithms: A survey. *computer*, 27(6):17–26, 1994.
- [51] Seyedali Mirjalili, Jin Song Dong, Ali Safa Sadiq, and Hossam Faris. Genetic algorithm: Theory, literature review, and application in image reconstruction. In *Nature-Inspired Optimizers*, pages 69–85. Springer, 2020.
- [52] Jonas Mockus, Vytautas Tiesis, and Antanas Zilinskas. The application of bayesian methods for seeking the extremum. *Towards global optimization*, 2(117-129):2, 1978.
- [53] Harold J Kushner. A new method of locating the maximum point of an arbitrary multipeak curve in the presence of noise. *Journal of Basic Engineering*, 86(1):97–106, 1964.
- [54] Bobak Shahriari, Kevin Swersky, Ziyu Wang, Ryan P Adams, and Nando De Freitas. Taking the human out of the loop: A review of bayesian optimization. *Proceedings of the IEEE*, 104(1):148–175, 2015.

- [55] Donald R Jones. A taxonomy of global optimization methods based on response surfaces. *Journal of global optimization*, 21(4):345–383, 2001.
- [56] Matthias Feurer, Aaron Klein, Katharina Eggersperger, Jost Springenberg, Manuel Blum, and Frank Hutter. Methods for improving bayesian optimization for automl. In *Proceedings of the International Conference on Machine Learning*, 2015.
- [57] Chris Thornton, Frank Hutter, Holger H Hoos, and Kevin Leyton-Brown. Auto-weka: Combined selection and hyperparameter optimization of classification algorithms. In *Proceedings of the 19th ACM SIGKDD international conference on Knowledge discovery and data mining*, pages 847–855, 2013.
- [58] Kevin Swersky, Jasper Snoek, and Ryan P Adams. Multi-task bayesian optimization. In *Advances in neural information processing systems*, pages 2004–2012, 2013.
- [59] Julius von Kügelgen, Paul K Rubenstein, Bernhard Schölkopf, and Adrian Weller. Optimal experimental design via bayesian optimization: active causal structure learning for gaussian process networks. *arXiv preprint arXiv:1910.03962*, 2019.
- [60] Adam Foster, Martin Jankowiak, Elias Bingham, Paul Horsfall, Yee Whye Teh, Thomas Rainforth, and Noah Goodman. Variational bayesian optimal experimental design. In *Advances in Neural Information Processing Systems*, pages 14036–14047, 2019.
- [61] Joep Vanlier, Christian A Tiemann, Peter AJ Hilbers, and Natal AW van Riel. A bayesian approach to targeted experiment design. *Bioinformatics*, 28(8):1136–1142, 2012.
- [62] Carl Edward Rasmussen. Gaussian processes in machine learning. In *Summer School on Machine Learning*, pages 63–71. Springer, 2003.
- [63] Leo Breiman. Random forests. *Machine learning*, 45(1):5–32, 2001.
- [64] Jasper Snoek, Oren Rippel, Kevin Swersky, Ryan Kiros, Nadathur Satish, Narayanan Sundaram, Mostofa Patwary, Mr Prabhat, and Ryan Adams. Scalable bayesian optimization using deep neural networks. In *International conference on machine learning*, pages 2171–2180, 2015.
- [65] Donald R Jones, Matthias Schonlau, and William J Welch. Efficient global optimization of expensive black-box functions. *Journal of Global optimization*, 13(4):455–492, 1998.
- [66] Niranjan Srinivas, Andreas Krause, Sham M Kakade, and Matthias W Seeger. Information-theoretic regret bounds for gaussian process optimization in the bandit setting. *IEEE Transactions on Information Theory*, 58(5):3250–3265, 2012.
- [67] José Miguel Hernández-Lobato, Matthew W Hoffman, and Zoubin Ghahramani. Predictive entropy search for efficient global optimization of black-box functions. In *Advances in neural information processing systems*, pages 918–926, 2014.
- [68] Florian Häse, Loïc M Roch, Christoph Kreisbeck, and Alán Aspuru-Guzik. Phoenix: A bayesian optimizer for chemistry. *ACS central science*, 4(9):1134–1145, 2018.
- [69] Daniel Golovin, Benjamin Solnik, Subhdeep Moitra, Greg Kochanski, John Karro, and D Sculley. Google vizier: A service for black-box optimization. In *Proceedings of the 23rd ACM SIGKDD International Conference on Knowledge Discovery and Data Mining*, pages 1487–1495. ACM, 2017.
- [70] The GPyOpt authors. Gpyopt: A bayesian optimization framework in python. <http://github.com/SheffieldML/GPyOpt>, 2016.
- [71] Eduardo C Garrido-Merchán and Daniel Hernández-Lobato. Dealing with categorical and integer-valued variables in bayesian optimization with gaussian processes. *Neurocomputing*, 2019.
- [72] José Miguel Hernández-Lobato, James Requeima, Edward O Pyzer-Knapp, and Alán Aspuru-Guzik. Parallel and distributed thompson sampling for large-scale accelerated exploration of chemical space. In *Proceedings of the 34th International Conference on Machine Learning-Volume 70*, pages 1470–1479. JMLR. org, 2017.
- [73] Kai Wang Ng, Guo-Liang Tian, and Man-Lai Tang. *Dirichlet and related distributions: Theory, methods and applications*, volume 888. John Wiley & Sons, 2011.
- [74] J Atchison and Sheng M Shen. Logistic-normal distributions: Some properties and uses. *Biometrika*, 67(2):261–272, 1980.
- [75] Diederik P Kingma and Max Welling. Auto-encoding variational bayes. *arXiv preprint arXiv:1312.6114*, 2013.
- [76] Chris J Maddison, Andriy Mnih, and Yee Whye Teh. The concrete distribution: A continuous relaxation of discrete random variables. *arXiv preprint arXiv:1611.00712*, 2016.
- [77] Eric Jang, Shixiang Gu, and Ben Poole. Categorical reparameterization with gumbel-softmax. *arXiv preprint arXiv:1611.01144*, 2016.
- [78] Stuart Geman, Elie Bienenstock, and René Doursat. Neural networks and the bias/variance dilemma. *Neural computation*, 4(1):1–58, 1992.
- [79] Christoph Molnar. *Interpretable machine learning*. Lulu.com, 2019.
- [80] F. Häse, L. M. Roch, and A. Aspuru-Guzik. Gryffin: An algorithm for bayesian optimization for categorical variables informed by physical intuition with applications to chemistry. *GitHub*, <https://github.com/aspuru-guzik-group/gryffin>, 2019.
- [81] Christian S Perone. Pyevolve: a python open-source framework for genetic algorithms. *ACM Sigevolution*, 4(1):12–20, 2009.
- [82] M. Lindauer, K. Eggersperger, M. Feurer, S. Falkner, A. Biedenkapp, and F. Hutter. Smac v3: Algorithm configuration in python. <https://github.com/automl/SMAC3>, 2017.
- [83] F. Hutter, H. H. Hoos, and K. Leyton-Brown. Parallel algorithm configuration. *Learn. Intell. Optim.*, pages 55–70, 2012.
- [84] F. Hutter, H. H. Hoos, and K. Leyton-Brown. Sequential model-based optimization for general algorithm configuration. In *International Conference on Learning and Intelligent Optimization*, pages 507–523. Springer, 2011.
- [85] Javier González, Michael Osborne, and Neil D Lawrence. Glasses: Relieving the myopia of bayesian optimisation. 2016.
- [86] Javier González, Zhenwen Dai, Philipp Hennig, and Neil Lawrence. Batch bayesian optimization via local penalization. In *Artificial Intelligence and Statistics*, pages 648–657, 2016.
- [87] Javier Gonzalez, Joseph Longworth, David C James, and Neil D Lawrence. Bayesian optimization for synthetic gene design. *arXiv preprint arXiv:1505.01627*, 2015.
- [88] J. S. Bergstra, D. Yamins, and D. D. Cox. Making a

- science of model search: Hyperparameter optimization in hundreds of dimensions for vision architectures. 2013.
- [89] J. S. Bergstra, R. Bardenet, Y. Bengio, and B. Kégl. Algorithms for hyper-parameter optimization. In *Advances in neural information processing systems*, pages 2546–2554, 2011.
- [90] Richard E Bellman. *Adaptive control processes: a guided tour*, volume 2045. Princeton university press, 2015.
- [91] Florian Häse, Loïc M Roch, and Alán Aspuru-Guzik. Chimera: enabling hierarchy based multi-objective optimization for self-driving laboratories. *Chemical Science*, 9(39):7642–7655, 2018.
- [92] Cengqi Yan, Stephen Barlow, Zhaohui Wang, He Yan, Alex K-Y Jen, Seth R Marder, and Xiaowei Zhan. Non-fullerene acceptors for organic solar cells. *Nature Reviews Materials*, 3(3):18003, 2018.
- [93] Jianhui Hou, Olle Inganäs, Richard H Friend, and Feng Gao. Organic solar cells based on non-fullerene acceptors. *Nature materials*, 17(2):119, 2018.
- [94] Steven A Lopez, Benjamin Sanchez-Lengeling, Julio de Goes Soares, and Alan Aspuru-Guzik. Design principles and top non-fullerene acceptor candidates for organic photovoltaics. *Joule*, 1(4):857–870, 2017.
- [95] M. J. Frisch, G. W. Trucks, H. B. Schlegel, G. E. Scuseria, M. A. Robb, J. R. Cheeseman, G. Scalmani, V. Barone, G. A. Petersson, H. Nakatsuji, X. Li, M. Caricato, A. V. Marenich, J. Bloino, B. G. Janesko, R. Gomperts, B. Mennucci, H. P. Hratchian, J. V. Ortiz, A. F. Izmaylov, J. L. Sonnenberg, D. Williams-Young, F. Ding, F. Lipparini, F. Egidi, J. Goings, B. Peng, A. Petrone, T. Henderson, D. Ranasinghe, V. G. Zakrzewski, J. Gao, N. Rega, G. Zheng, W. Liang, M. Hada, M. Ehara, K. Toyota, R. Fukuda, J. Hasegawa, M. Ishida, T. Nakajima, Y. Honda, O. Kitao, H. Nakai, T. Vreven, K. Throssell, J. A. Montgomery, Jr., J. E. Peralta, F. Ogliaro, M. J. Bearpark, J. J. Heyd, E. N. Brothers, K. N. Kudin, V. N. Staroverov, T. A. Keith, R. Kobayashi, J. Normand, K. Raghavachari, A. P. Rendell, J. C. Burant, S. S. Iyengar, J. Tomasi, M. Cossi, J. M. Millam, M. Klene, C. Adamo, R. Cammi, J. W. Ochterski, R. L. Martin, K. Morokuma, O. Farkas, J. B. Foresman, and D. J. Fox. Gaussian16 Revision C.01, 2016. Gaussian Inc. Wallingford CT.
- [96] Harikrishna Sahu, Weining Rao, Alessandro Troisi, and Haibo Ma. Toward predicting efficiency of organic solar cells via machine learning and improved descriptors. *Advanced Energy Materials*, 8(24):1801032, 2018.
- [97] Vishwesh Venkatraman and Bjørn Kåre Alsberg. A quantitative structure-property relationship study of the photovoltaic performance of phenothiazine dyes. *Dyes and Pigments*, 114:69–77, 2015.
- [98] Markus C Scharber, David Mühlbacher, Markus Koppe, Patrick Denk, Christoph Waldauf, Alan J Heeger, and Christoph J Brabec. Design rules for donors in bulk-heterojunction solar cellstowards 10% energy-conversion efficiency. *Advanced materials*, 18(6):789–794, 2006.
- [99] Markus C Scharber, David Mühlbacher, Markus Koppe, Patrick Denk, Christoph Waldauf, Alan J Heeger, and Christoph J Brabec. Design rules for donors in bulk-heterojunction solar cellstowards 10% energy-conversion efficiency. *Advanced materials*, 18(6):789–794, 2006.
- [100] Tayebbeh Ameri, Gilles Dennler, Christoph Lungen-schmied, and Christoph J Brabec. Organic tandem solar cells: A review. *Energy & Environmental Science*, 2(4):347–363, 2009.
- [101] Nam Joong Jeon, Jun Hong Noh, Woon Seok Yang, Young Chan Kim, Seungchan Ryu, Jangwon Seo, and Sang Il Seok. Compositional engineering of perovskite materials for high-performance solar cells. *Nature*, 517(7535):476, 2015.
- [102] Woon Seok Yang, Jun Hong Noh, Nam Joong Jeon, Young Chan Kim, Seungchan Ryu, Jangwon Seo, and Sang Il Seok. High-performance photovoltaic perovskite layers fabricated through intramolecular exchange. *Science*, 348(6240):1234–1237, 2015.
- [103] Wanyi Nie, Hsinhan Tsai, Reza Asadpour, Jean-Christophe Blancon, Amanda J Neukirch, Gautam Gupta, Jared J Crochet, Manish Chhowalla, Sergei Tretiak, Muhammad A Alam, et al. High-efficiency solution-processed perovskite solar cells with millimeter-scale grains. *Science*, 347(6221):522–525, 2015.
- [104] Hairen Tan, Ankit Jain, Oleksandr Voznyy, Xinzhen Lan, F Pelayo García De Arquer, James Z Fan, Rafael Quintero-Bermudez, Mingjian Yuan, Bo Zhang, Yicheng Zhao, et al. Efficient and stable solution-processed planar perovskite solar cells via contact passivation. *Science*, 355(6326):722–726, 2017.
- [105] C. Kim, T. D. Huan, S. Krishnan, and R. Ramprasad. A hybrid organic-inorganic perovskite dataset. *Sci. Data*, 4:170057, 2017.
- [106] Jongseob Kim, Sung-Hoon Lee, Choong-Heui Chung, and Ki-Ha Hong. Systematic analysis of the unique band gap modulation of mixed halide perovskites. *Physical Chemistry Chemical Physics*, 18(6):4423–4428, 2016.
- [107] Jongseob Kim, Seung-Cheol Lee, Sung-Hoon Lee, and Ki-Ha Hong. Importance of orbital interactions in determining electronic band structures of organo-lead iodide. *The Journal of Physical Chemistry C*, 119(9):4627–4634, 2015.
- [108] Paolo Umari, Edoardo Mosconi, and Filippo De Angelis. Relativistic gw calculations on ch 3 nh 3 pbi 3 and ch 3 nh 3 sni 3 perovskites for solar cell applications. *Scientific reports*, 4:4467, 2014.
- [109] Giacomo Giorgi, Jun-Ichi Fujisawa, Hiroshi Segawa, and Koichi Yamashita. Cation role in structural and electronic properties of 3d organic-inorganic halide perovskites: a dft analysis. *The Journal of Physical Chemistry C*, 118(23):12176–12183, 2014.
- [110] James Endres, David A Egger, Michael Kulbak, Ross A Kerner, Lianfeng Zhao, Scott H Silver, Gary Hodes, Barry P Rand, David Cahen, Leeor Kronik, et al. Valence and conduction band densities of states of metal halide perovskites: a combined experimental-theoretical study. *The journal of physical chemistry letters*, 7(14):2722–2729, 2016.
- [111] Norio Miya. Metal-catalyzed cross-coupling reactions of organoboron compounds with organic halides. *Metal-Catalyzed Cross-Coupling Reactions*, pages 41–123, 2004.
- [112] Dean G Brown and Jonas Bostrom. Analysis of past and present synthetic methodologies on medicinal chemistry: where have all the new reactions gone? miniperspective. *Journal of medicinal chemistry*, 59(10):4443–4458, 2015.

## Supplementary Information

### S.1. FORMULATING GRYFFIN

In the following, we detail the derivation of the three variants of GRYFFIN for the descriptor-guided optimization of categorical variables.

#### A. Deriving kernel based Bayesian optimization for categorical variables

The naïve GRYFFIN approach for the optimization of categorical variables follows the recently introduced PHOENICS strategy, which combines Bayesian kernel density estimation with Bayesian optimization for continuous parameter domains.<sup>1</sup> PHOENICS is based on the idea that kernel densities of evaluated parameters can indicate promising regions in the parameter space where the global optimum could (not) be located based on the response values observed for the evaluated parameters. The naïve GRYFFIN approach extends this idea to categorical parameter spaces.

PHOENICS models kernel densities on continuous domains with normal priors, where the parameters of the normal priors are sampled from a Bayesian neural network conditioned on the observed parameter points. The use of normal priors serves two purposes: (i) the locations and the precisions of the priors can be controlled independently, (ii) the priors can be reparameterized into deterministic functions of their parameters and stationary noise nodes. With the first purpose, the priors can be fine tuned based on the collected observations, while the latter purpose accelerates computations for inference and predictions in automatic differentiation frameworks.<sup>2</sup>

The generalization of kernel density augmented Bayesian optimization to categorical parameters requires kernel density priors which satisfy these two criteria. One potential candidate is the recently introduced concrete distribution<sup>3</sup> (simultaneously introduced as Gumbel-Softmax)<sup>4</sup> which is defined on the  $n$ -dimensional simplex  $\Delta^{n-1}$ , defined by  $\mathbf{z} \in \Delta^{n-1} = \{\mathbf{z} \in \mathbb{R}^n | z_i \in [0, 1] \text{ and } \sum_{i=1}^n z_i = 1\}$ , with the probability distribution

$$p_{\pi, \tau}(\mathbf{z}) = \Gamma(n)\tau^{n-1} \prod_{k=1}^n \left( \frac{\pi z_k^{-\tau-1}}{\sum_{i=1}^n \pi z_i^{-\tau}} \right), \quad (3)$$

where  $\tau$  is a temperature parameter which controls the precision of the distribution, and  $\pi$  indicate the class probabilities. Samples  $\mathbf{z}$  of the concrete distribution can be generated by sampling from a standard Gumbel distribution, i.e. we draw i.i.d. samples  $g_k \sim \text{Gumbel}(0, 1)$ , and setting

$$z_k = \frac{\exp((\log \pi + g_k)/\tau)}{\sum_{i=1}^n \exp((\log \pi + g_i)/\tau)}. \quad (4)$$

Note, that the parameters  $\pi$  are deterministic. Based on the kernel densities  $p_k(\mathbf{z})$  and the associated observed responses  $f_k$ , where  $k$  indicates the  $k$ -th measurement, we can construct the acquisition function

$$\alpha(\mathbf{z}) = \frac{\sum_{k=1}^n f_k p_k(\mathbf{z}) + \lambda p_{\text{uniform}}(\mathbf{z})}{\sum_{k=1}^n p_k(\mathbf{z}) + p_{\text{uniform}}(\mathbf{z})}, \quad (5)$$

where  $\lambda$  is a sampling parameter which controls the degree of exploitation or exploration expressed by the acquisition function.<sup>1</sup> New parameter points for future evaluations are suggested based on the location of the global optimum of this acquisition function, where  $\lambda$  tunes the behavior of this acquisition function from a bias towards exploration ( $\lambda \ll 0$ ) to a bias towards exploitation ( $\lambda \gg 0$ ). The global optimum of the acquisition function is located based on random sampling with a local refinement of promising candidates using L-BFGS.<sup>5</sup>

#### B. Enabling descriptor-guided optimizations on categorical spaces

The static GRYFFIN approach extends the categorical optimization strategy detailed in Sec. S.1.A to cases where individual options of a categorical variable  $\mathbf{z}$  can be associated to a set of descriptors  $\mathbf{x}$ , for which we can define a metric to measure their pairwise distances. For simplicity, we consider the case that descriptors are  $m$ -dimensional real-valued vectors,  $\mathbf{x} \in \mathbb{R}^m$ , for which we compute distances following the Euclidean norm. We further assume that the descriptors are uniquely associated with individual options, such that no two options are described by the same descriptor.

While options for future evaluations could be selected directly from the real valued space  $\mathbb{R}^m$  in which the descriptors are embedded, the efficient selection of candidates solely based on their descriptors is non-trivial for various reasons. For example, the geometry of the descriptors embedded in the real space is unknown and can be highly complex for a generic optimization task, which poses a challenge to defining domain boundaries. Furthermore, only specific points in the descriptor space correspond to realizable options of the categorical variable, such that the selection of the next candidate to evaluate can be ambiguous. To avoid these challenges, static GRYFFIN instead suggests new options based on kernel densities constructed on the categorical space, where the geometry of the space is known. Static GRYFFIN accounts for descriptor information by locally transforming the metric on the categorical space based on varying distances between individual descriptors. To this end, static GRYFFIN constructs a metric tensor for the categorical space from the descriptors associated with individual options.

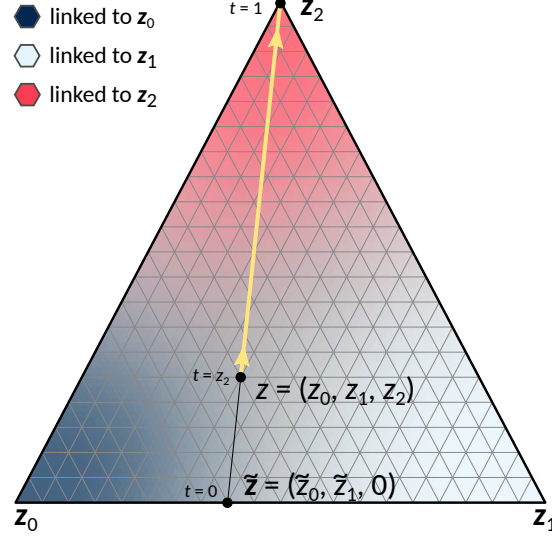


FIG. S.7: Illustration of the path in the categorical space along which changes of a given descriptor are computed for a change in a given categorical option. The path is parameterized by  $t$  and goes from  $\mathbf{z}$  to  $\mathbf{z}_2$  in this example.

In the following, we derive an expression for the distance between any point  $\mathbf{z}$  on a simplex with dimensionality  $\#opt$  and a particular target corner,  $\mathbf{z}_t = \delta_{it}\mathbf{e}_i$  for  $i = 0, \dots, \#opt$ , computed based on the metric spanned by the descriptors associated with individual options, following the example illustrated in Fig. S.7. The infinitesimal line element on the descriptor space with  $\#desc$ -many descriptors can be calculated following the Euclidean norm

$$ds^2 = \sum_{m=1}^{\#desc} dx_m dx_m, \quad (6)$$

where we sum over all descriptors. With the assumption that descriptors are a function of the points on the simplex,  $\mathbf{x} = \mathbf{x}(\mathbf{z})$ , we can compute the infinitesimal changes in the descriptors via infinitesimal changes in the categorical variable

$$dx_m = \sum_{i=1}^{\#opt} \frac{\partial x_m}{\partial z_i} dz_i. \quad (7)$$

The infinitesimal line element  $ds$  can then be expressed as

$$ds^2 = \sum_{m=1}^{\#desc} \sum_{i,j=1}^{\#opt} \frac{\partial x_m}{\partial z_i} \frac{\partial x_m}{\partial z_j} dz_i dz_j \quad (8)$$

Further, if we assume that  $\mathbf{x}(\mathbf{z})$  is a linear function of the points on the simplex, we can replace  $dx \rightarrow \Delta x$ ,  $dz \rightarrow \Delta z$  and  $ds \rightarrow \Delta s$ . The length of the path from a point  $\mathbf{z}$  on the simplex to the corner  $\mathbf{z}_i$  then simplifies to

$$\Delta s^2 = \sum_{m=1}^{\#desc} \sum_{i,j=1}^{\#opt} \frac{\Delta x_m}{\Delta z_i} \frac{\Delta x_m}{\Delta z_j} \Delta z_i \Delta z_j = \sum_{m=1}^{\#desc} \sum_{i,j=1}^{\#opt} \Delta x_m^i \Delta x_m^j, \quad (9)$$



where we introduced  $\Delta x_m^i$  to describe the change of the  $m$ -th descriptor with a change in the  $i$ -th option of the categorical variable. To compute this change in the descriptor, we consider a straight line in the categorical space as illustrated in Fig. S.7.

$$\mathbf{z}(t) = (1-t)\tilde{\mathbf{z}} + t\mathbf{z}_i, \quad \text{where } t \in [0, 1] \quad (10)$$

and compute the value of the descriptor  $\mathbf{x}_m$  along this path. For  $t = 1$ , the value of  $\mathbf{x}_m$  is identical to the value of the  $m$ -th descriptor of the  $i$ -th categorical option. For  $t = 0$ , however, the value of  $\mathbf{x}_m$  is given by the weighted average of the descriptors  $x_m$  across all categories but the  $i$ -th category.

$$x_m(t=0) = \sum_{k \neq i}^{\# \text{opt}} \frac{z_k}{1-z_i} x_m^{\text{opt}_k}, \quad x_m(t=1) = x_m^{\text{opt}_i} \quad (11)$$

Hence, for a given point  $\mathbf{z}$  along this path,

$$x_m(\mathbf{z}) = z_i x_m^{\text{opt}_i} + (1-z_i) \sum_{k \neq i}^{\# \text{opt}} \frac{z_k}{1-z_i} x_m^{\text{opt}_k} \quad (12)$$

where  $x_m^{\text{opt}_i}$  denotes the value of the  $m$ -th descriptor of the  $i$ -th categorical option. Following the path from  $\mathbf{z}$  to  $\mathbf{z}_i$  (yellow line in Fig. S.7), we find that  $x_m$  changes as

$$\Delta x_m^i = x_m^{\text{opt}_i} - \sum_{k=1}^{\# \text{opt}} z_k x_m^{\text{opt}_k} \quad (13)$$

We then compute the length of the path outlined in Fig. S.7 to arrive at

$$\begin{aligned} \Delta s^2 &= \sum_{m=1}^{\# \text{desc}} \sum_{i,j=1}^{\# \text{opt}} \left( x_m^{\text{opt}_i} - \sum_{k=1}^{\# \text{opt}} z_k x_m^{\text{opt}_k} \right) \left( x_m^{\text{cat}_i} - \sum_{k=1}^{\# \text{opt}} z_k x_m^{\text{opt}_k} \right) \\ &= (\# \text{opt})^2 \sum_{m=1}^{\# \text{desc}} \left( x_m^{\text{opt}_i} - \sum_{k=1}^{\# \text{opt}} z_k x_m^{\text{opt}_k} \right) \left( x_m^{\text{opt}_i} - \sum_{k=1}^{\# \text{opt}} z_k x_m^{\text{opt}_k} \right) \end{aligned} \quad (14)$$

Eq. 14 presents the final equation to recompute distances. Based on these distances, similarity between sampled points on the simplex and its corners can be established.

The reshaping process is further illustrated on a three dimensional categorical space in Fig. S.8 for two different sets of descriptors. Fig. S.8a is generated for a set of three dimensional descriptors with equal pairwise distances between them, with  $x_0 = (1, 0, 0)$ ,  $x_1 = (0, 1, 0)$  and  $x_2 = (0, 0, 1)$ , while Fig. S.8b,c are generated for descriptors with different pairwise distances arising from  $x_0 = (1, 1, 1)$ ,  $x_1 = (1/4, 1, 1/2)$  and  $x_2 = (0, 0, 1)$ . Panels (i) are created with the Euclidean metric on the simplex, such that the color contours in panels (a.i) and (a.ii) illustrate the closest corner point to any point in the simplex, and (a.iii) shows an arbitrary kernel density sampled from a concrete distribution. The meshes illustrate line elements of equal length along individual coordinates. Panels (ii) show the meshes computed for the descriptor-guided metric, while contour plots follow the Euclidean metric. Panels (iii) show the contours for the descriptor-guided metric and the meshes for the Euclidean metric.

### C. Data-driven construction of more informative descriptors

Static GRYFFIN leverages real-valued descriptors to navigate categorical spaces in search for the best performing options. Such descriptor-guided searches, however, can only achieve faster optimization rates if the provided descriptors are representative of the expected performance of individual options. In fact, for an optimal performance of static GRYFFIN, the provided descriptors should perfectly correlate with the collected measurements, which will rarely be the case in real-world applications. However, descriptors which only poorly resemble the associated measurements cannot efficiently guide the search.

The dynamic GRYFFIN approach aims to alleviate this limitation by constructing more informative descriptors, denoted with  $\mathbf{x}'$  on-the-fly from the responses  $\{f_k\}$  collected during the optimization and the provided descriptors  $\mathbf{x}$ . The transformed descriptors  $\mathbf{x}'$  are considered to be more informative if they achieve higher correlations with the

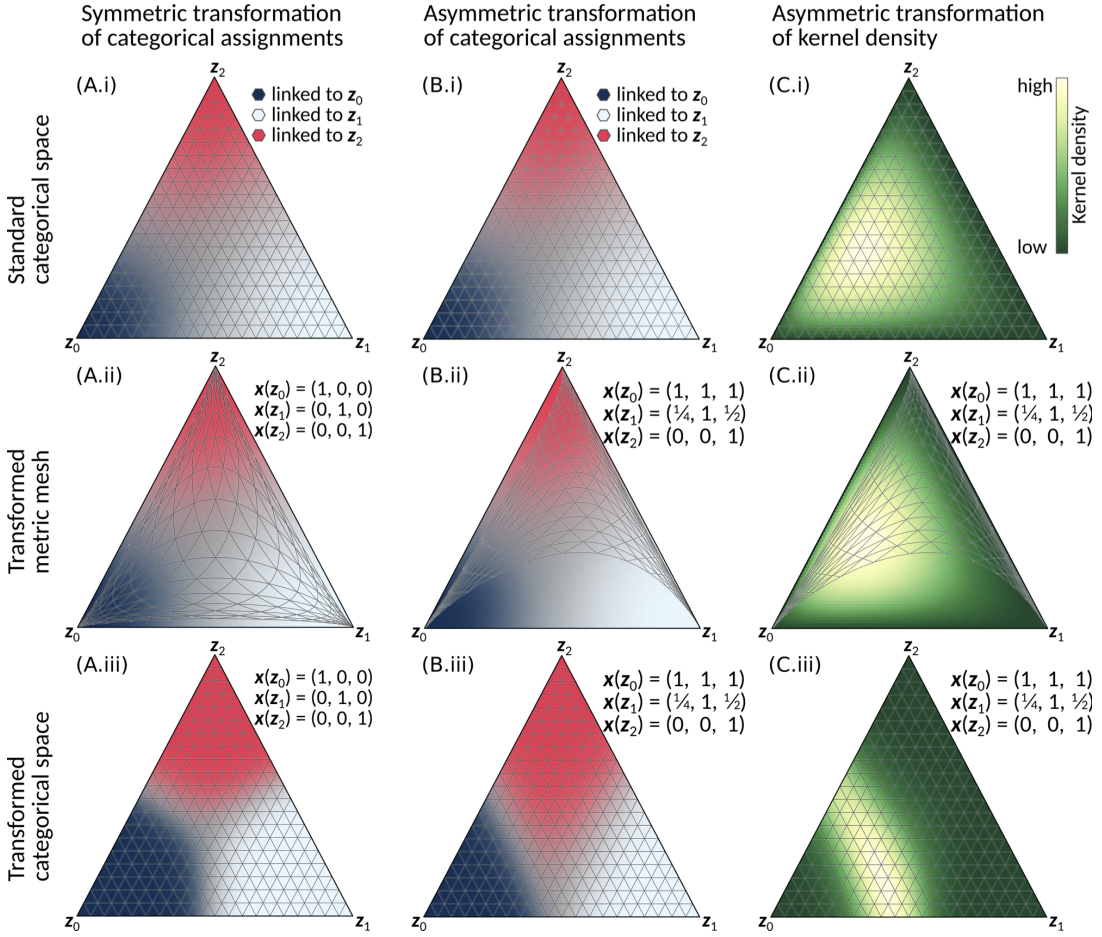


FIG. S.8: Illustration of a three dimensional categorical space, where a metric is defined based on the Euclidean norm between descriptors associated to the options of the categorical space (in comparison to a Euclidean metric on the categorical space). (A): Illustration of a descriptor-guided metric with equidistant descriptors. Color contours indicate the closest options. (B): Illustration of a descriptor-guided metric with arbitrary descriptors. Color contours indicate the closest option (C): Illustration of the transformation of a kernel density on the categorical space based on the metric imposed by the descriptors used in panels (B). Color contours depict the kernel density. Panels (i) highlight contours and meshes on the simplex with a Euclidean norm. Panels (ii) illustrate meshes for the descriptor-guided metric on color contours for the Euclidean norm. Panels (iii) show color contours for the descriptor-guided metric with meshes represented in the Euclidean norm.

collected measurements  $\{f_k\}$ , which are quantified *via* the Pearson correlation coefficient. Note, that we focus on large Pearson correlations without loss of generality, as highly negative coefficients close to -1 can be converted to large coefficients by an irrelevant sign flip in the descriptors. The construction of a transformation  $T$ , which generates more informative descriptors  $\mathbf{x}'$  from the provided descriptors  $\mathbf{x}$ , i.e.  $T: \mathbf{x} \mapsto \mathbf{x}'$ , can potentially elucidate the relevance of the provided descriptors, measured by their significance and influence to the construction of  $\mathbf{x}'$ . As such, analyzing the transformation  $T$  and identifying the descriptors  $\mathbf{x}$  to which the measurements are most sensitive has the potential to inspire scientific insights.<sup>6</sup>

Dynamic GRYFFIN implements the descriptor transformation  $T$  targeting three goals.

- (i) Maximizing the correlation between collected measurements  $\{f_k\}$  and at least one of the transformed descriptors  $\mathbf{x}'_i$ . Transformed descriptors which highly correlate with the collected measurements can efficiently guide an optimization strategy such as GRYFFIN, as demonstrated in Sec. IV of the main text.
- (ii) Reducing the cardinality of the set of transformed descriptors, such that only informative descriptors are retained. Larger sets of descriptors are more likely to span highly non-linear manifolds with stronger local curvatures, which can pose challenges to efficient optimizations.
- (iii) Reducing the pairwise correlation between any two transformed descriptors. Two highly correlated descriptors contain redundant information which is irrelevant for the optimization. The set of transformed descriptors is most informative if there is little correlation between any two transformed descriptors.

### 1. Defining the class of suitable transformations

We model the transformation  $T$  by a slightly non-linear operation, which could be interpreted as a simple, one-layer neural network. Specifically, we construct  $T$  following Eq. 15, where  $\mathbf{W}$  and  $\mathbf{b}$  are trainable parameters inferred from the collected measurements.

$$\mathbf{x}' = T(\mathbf{x}; \mathbf{W}, \mathbf{b}) = \text{softsign}(\mathbf{W} \cdot \mathbf{x} + \mathbf{b}), \quad \text{where} \quad \text{softsign}(x) = \frac{x}{1 + |x|} \quad (15)$$

This model architecture encodes slightly non-linear translations and rotations on the descriptor space. Although the simplicity of this model restricts the possible set of transformations, it substantially reduces the risk of overfitting on the low-data regimes commonly encountered in autonomous experimentation workflows. In addition, linear regression models are typically easier to interpret than more elaborate models with more complicated architectures, such that this choice of  $T$  can potentially facilitate scientific insights. The architecture and the effect of realizable transformations on the descriptors are illustrated in Fig. S.9.

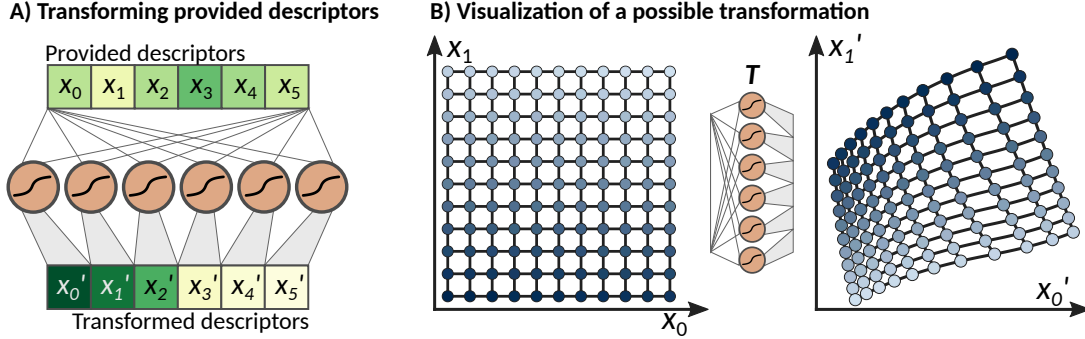


FIG. S.9: Illustration of the transformation  $T$  leveraged by dynamic GRYFFIN to learn a more informative set of descriptors from collected measurements. (A) Architecture of the transformation, illustrated as a single-layer neural network. (B) Possible transformations spanned by the network architecture.

### 2. Data-driven construction of suitable transformations

The parameters  $\mathbf{W}$  and  $\mathbf{b}$  of the transformation  $T$  described by Eq. 15 are inferred from collected measurements to satisfy the three aforementioned goals. To this end, we define a set of penalties,  $\lambda$ , which are collectively minimized during inference via stochastic gradient descent. The first penalty,  $\lambda_0$ , targets the maximization of the correlation between at least one of  $n$  transformed descriptors and the collected measurements

$$\lambda_0 = 1 - \max_{0 \leq i \leq n} |\rho(x'_{i,k}, f_k)|, \quad (16)$$

where  $\rho(x'_{i,k}, f_k)$  denotes the Pearson correlation coefficient defined as

$$\rho(x'_{i,k}, f_k) = \frac{\mathbb{E}[(x'_{i,k} - \mu_{x'})(f_k - \mu_f)]}{\sigma_{x'} \sigma_f}, \quad (17)$$

and  $\mu$  and  $\sigma$  denote the mean and standard deviation of the descriptors and measurements over the set of all executed evaluations. Note, that this penalty favors correlation over anti-correlation without loss of generality. Given at least one highly correlated descriptor, the correlation between the measurements and all other descriptors should either be high (for the descriptor to be informative) or close to zero (for the descriptor to be insignificant). In the case of high correlation, the transformed descriptors will provide valuable information assuming little correlation between the transformed descriptors. Transformed descriptors with low correlations, however, can be neglected in the static GRYFFIN approach as they provide little guidance for the optimizer. To construct a penalty which reflects these two desired outcomes, we first estimate the expected values for insignificant correlations. Given two independent random sequences with  $n$  elements, the expected Pearson correlation coefficient  $\rho$  is zero with a standard error  $\Delta\rho$  of approximately

$$\Delta\rho = \frac{1}{\sqrt{n-3}}, \quad (18)$$

as derived by Fisher.<sup>7,8</sup> We consider a detected Pearson correlation as significant, if it is above the expected standard error, and define the adjusted correlation  $\tilde{\rho}$  as

$$\tilde{\rho} = \max \left( \frac{|\rho| - \Delta\rho}{1 - \Delta\rho}, 0 \right). \quad (19)$$

The second penalty is constructed from this adjusted correlation to equally favor correlations close to 1 or below the significance threshold

$$\lambda_1 = \frac{1}{n} \sum_{0 < i \leq n} \sin^2 \left( \pi \tilde{\rho}(x'_{i,k}, f_k) \right). \quad (20)$$

Our third penalty aims to decorrelate the transformed descriptors  $\mathbf{x}$  to diversify the information carried by each of the relevant descriptors. Indeed, transformed descriptors which all perfectly correlate with the collected measurements also necessarily correlate with one another, and are thus redundant. In the definition of this third penalty, we again consider correlations to be insignificant if they are below the threshold defined in Eq. 18

$$\lambda_2 = \frac{1}{n(n-1)} \sum_{\substack{0 < i, j \leq n \\ i \neq j}} \sin^2 \left( \frac{\pi}{2} \tilde{\rho}(x'_{i,k}, x'_{j,k}) \right). \quad (21)$$

Finally, the parameters  $\mathbf{W}$  of the transformation are  $L1$ -regularized to favor sparse operations which are easier to interpret. The regularization factor is denoted with  $\nu$  and set to  $10^{-3}$  in all experiments

$$\lambda_3 = \nu \sum_i |w_i|. \quad (22)$$

The overall penalty function

$$\lambda = \lambda_0 + \lambda_1 + \lambda_2 + \lambda_3, \quad (23)$$

is then minimized via stochastic gradient descent until no significant improvement is observed over a period of 20 epochs, or a total training duration of 1,000 epochs has been reached.

## S.2. SYNTHETIC BENCHMARK FUNCTIONS

We demonstrate the performance of the introduced formulations of GRYFFIN with empirical benchmarks conducted on a set of synthetic surfaces. The benchmark surfaces are constructed with inspiration drawn from well-established analytic functions on continuous spaces which are typically used to benchmark local and global optimization strategies. Specifically, we extend the widely used *ackley*, *camel*, *dejong* and *michalewicz* functions to categorical spaces with arbitrarily many categorical variables and options per variable. In addition, we introduce three partially and fully randomized surfaces, referred to as *slope* (no noise), *noise* (moderate noise) and *random* (purely random), where responses are perturbed by noise sampled from stationary uniform distributions. All benchmark surfaces are illustrated in the top panels of Fig. S.10 for two categorical variables with 21 options per variable.

It is important to note that there is no spatial relation between individual options since the order of any two options can be mutually switched without changing the surface. We illustrate this order ambiguity in the lower panels of Fig. S.10, where random permutations  $\pi$  have been performed on the *reference* order illustrated in the top panels to create the *shuffled* orders depicted in the lower panels. However, descriptors can be assigned to each of the categories such that a particular metric is imposed on the domain space. Unless noted otherwise, we use the *reference* ordering for all options when supplying descriptors to construct a metric space for these categorical benchmark functions.

In the following, we describe and characterize the introduced benchmark surfaces in more detail. Python implementations of the benchmark functions are made available on GitHub.<sup>9</sup>

*a. Ackley surface:* The *Ackley* surface is inspired by the Ackley path function for continuous spaces. It features a narrow funnel around the global minimum, which is degenerate if the number of options along one (or more) dimensions is even and well-defined if the number of options for all dimensions is odd.

*b. Camel surface:* The *Camel* surface is generalized from the Camel function on continuous domains and features a degenerate and *pseudo*-disconnected global minimum.

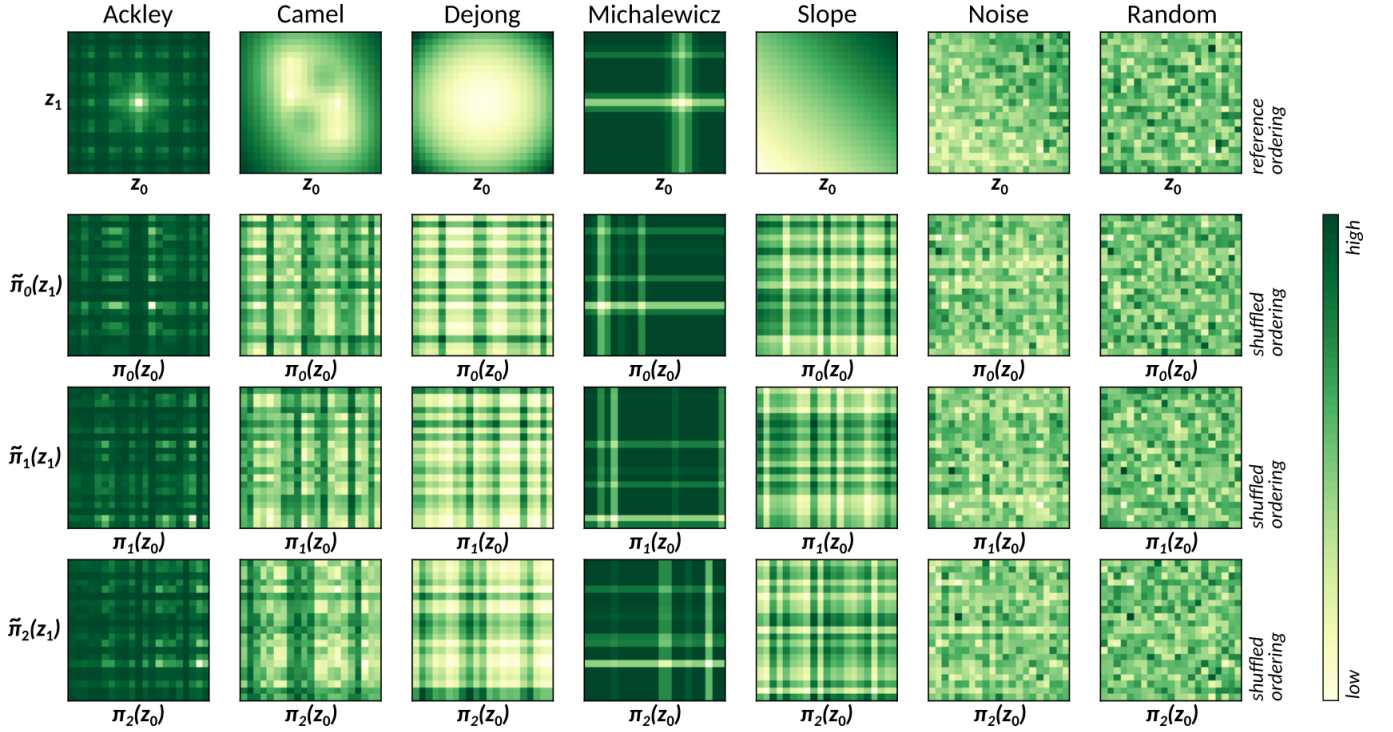


FIG. S.10: Synthetic benchmark functions generated for this study and employed for validating the introduced algorithm. The uppermost row depicts the benchmark functions in the *reference* ordering of the options available to each variable. The lower rows illustrate the shape of the benchmark functions for *shuffled* orderings generated from random permutations of the available options.

*c. Dejong surface:* The *Dejong* surface is inspired by the Dejong function and, as such, represents the generalization of a parabola to categorical spaces. We therefore refer to the *Dejong* functions as *pseudo-convex*. Similar to the *Ackley* surface, the *Dejong* surface features a well-defined global minimum if the number of options for all dimensions is odd, and a degenerate global minimum if at least one of the dimensions features an even number of options.

*d. Michalewicz surface:* The *Michalewicz* surface is generalized to categorical spaces from the Michalewicz function. This surface features well-defined options for each dimension which yield significantly better performances than others. In addition, the number of *pseudo-local* minima scales factorially with the number of dimensions.

*e. Slope surface:* The *Slope* surface is constructed such that the response linearly increases with the index of the option along each dimension in the reference ordering. As such, the *Slope* surface presents a generalization of a plane to categorical domains.

*f. Noise surface:* The *Noise* surface is a variant of the *Slope* surface, where perturbations sampled from a stationary uniform distribution are added to the responses of the surface, such that the overall correlation between the responses and the descriptors in the reference ordering target a Pearson correlation coefficient of 0.5. The noise added to the surface is fixed with a random seed conditioned on the dimensionality and the number of options per dimension, such that the surfaces are generated reproducibly.

*g. Random surface:* The *Random* surface is constructed from samples drawn from a stationary uniform distribution. To reproduce the surface, the random seed which generates the surface is conditioned on the dimensionality of the surface and the number of options per dimension.

### S.3. EMPIRICAL BENCHMARKS OF GRYFFIN ON SYNTHETIC SURFACES

In the following sections we empirically illustrate the performance of the three introduced variants of GRYFFIN on the synthetic benchmark surfaces introduced in Sec. S.2.

### A. Caching and boosting

The computationally most expensive step in the evaluation of the acquisition function is the computation of the kernel densities as an average over the number of samples drawn from the Bayesian neural network. However, the shape of the acquisition function is dominated by the (*a priori* known) uniform distribution in regions of the parameter space where the kernel densities assume relatively low values. Based on this observation, we suggest that the construction of the acquisition function can be accelerated with an approximate scheme, which estimates kernel density values from fewer samples in low density regions.

Following this strategy, we compute a first estimate to the value of the true kernel density  $p_{\text{true}}(\mathbf{z})$  at a given parameter point  $\mathbf{z}$  based on a randomly selected 10 % of the samples drawn from the Bayesian neural network. This preliminary estimate,  $p_{\text{approx},10}(\mathbf{z})$  is compared to the uniform distribution on the parameter domain,  $p_{\text{uniform}}(\mathbf{z})$ . If the estimated kernel density is greater than or equal to 1 % of the uniform distribution, i.e.

$$p_{\text{approx},10}(\mathbf{z}) \geq \frac{1}{100} p_{\text{uniform}}(\mathbf{z}), \quad (24)$$

the kernel density is considered to be sufficiently large to require a more accurate estimate,  $p_{\text{approx},100}$ , using 100 % of the samples. Otherwise, the evaluation is stopped and the more uncertain estimate is used to approximate the true kernel density, thus saving 90 % of the sample evaluations at this parameter point. Further accelerations of the implementation of the GRYFFIN framework are achieved by caching previously evaluated kernel densities to avoid redundant evaluations. Note, that this approach, however, balances reduced time requirements with slightly increased memory requirements and might thus not be applicable to all types of computational resources. We refer to this approximation as *pseudo-boosting*.

We empirically estimate the runtime accelerations and the degree of potential performance degradations due to approximations to the acquisition functions on six of the benchmark surfaces introduced in Sec. S.2. The performances of the *pseudo-boosting* strategy and the full sampling strategy are quantified based on the average best function values sampled for each benchmark surface after a certain number of iterations, while each optimization targets the location of the global minimum. Each benchmark surface is constructed with two categorical variables with 21 options per categorical variable. Results for 200 independent repetitions of the optimization runs for all surfaces are illustrated in Fig. S.11.

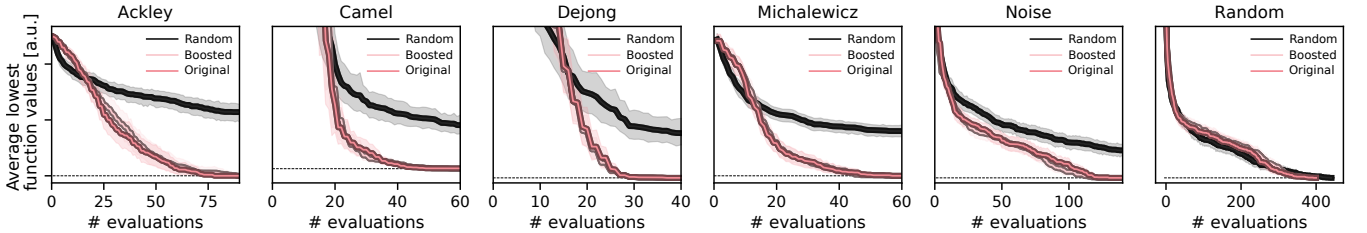


FIG. S.11: Performance of the pseudo-boosting and the full sampling formulations on six benchmark surfaces, averaged over 200 independent repetitions.

The benchmarks indicate no significant performance difference between the *pseudo-boosting* and the full sampling strategies of GRYFFIN, indicating that approximations to the acquisition function in low density regions does not severely affect the optimization runs. In addition to the performance, we also analyzed the computational time required for one iteration at a given number of options with fixed dimensionality (see Fig. S.12a), and varying number of parameters with a fixed number of options (see Fig. S.12a). All simulations were executed on an Intel(R) Core(TM) i5-7600K CPU at 3.8 GHz.

We find a linear dependence of the runtime with the number of observations in both cases. While the full sampling version of GRYFFIN experiences an increase in runtime of about 0.071 s with each additional observation, the increase in runtime of the pseudo-boosted version of GRYFFIN is about 0.028 s per observation and thus about 2.5 times slower. However, we do not observe any significant accelerations for a varying number of dimensions. We conclude that *pseudo-boosting* provides a runtime advantage when increasing the number of observations (as expected, by construction) without any noticeable degradations in the optimization performance. Based on these findings we recommend the *pseudo-boosted* version of GRYFFIN and use the *pseudo-boosted* version for all reported studies unless noted otherwise.



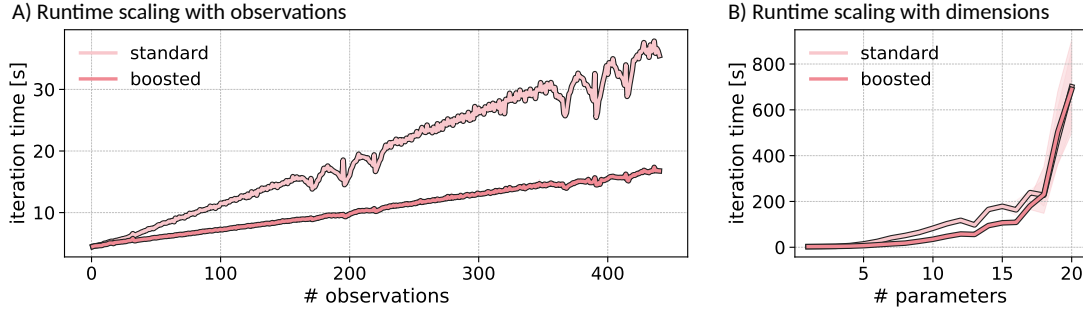


FIG. S.12: Illustrations of the computational scaling of GRYFFIN with and without *pseudo-boosting*. (A) two dimensional response surface with varying number of observations. (B) ten observations with varying response surface dimensionality.

### B. Traces of the analytic benchmarks

Fig. S.13 illustrates the traces of 200 independent optimization runs of each of the studied optimization strategies on four synthetic benchmark surfaces, supplementing the results reported in Sec. IV of the main text. Descriptors were provided in the reference ordering introduced in Sec. S.2.

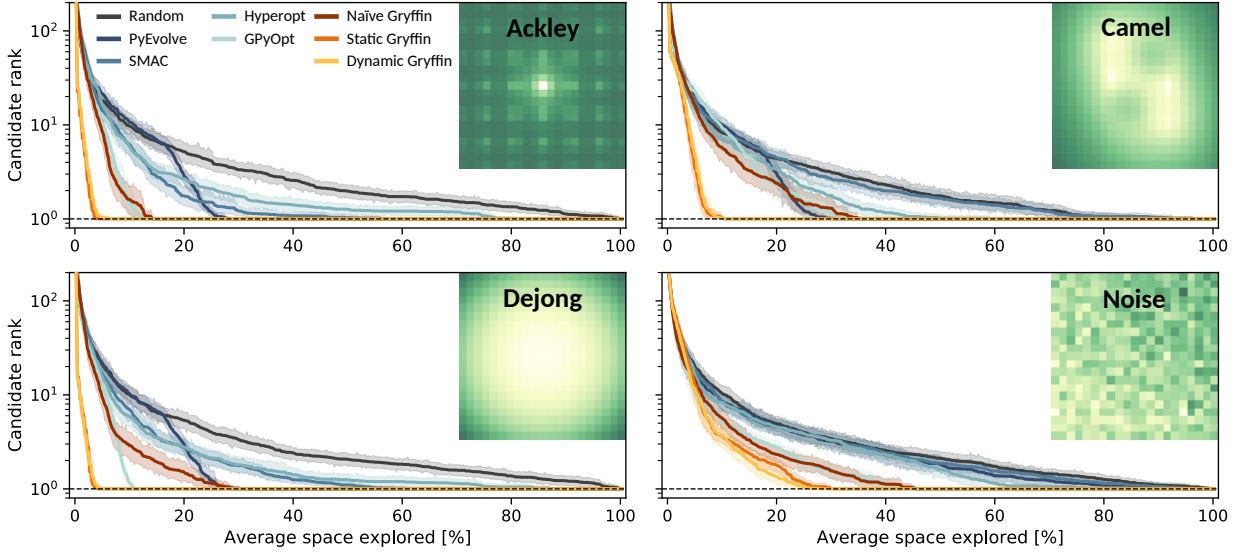


FIG. S.13: Average rank of the best performing candidate found by each of the studied optimization strategies in 200 independent optimization runs. Benchmark surfaces are illustrated in the reference ordering for two categorical variables with 21 options each.

### C. Influence of the number of dimensions

We empirically estimate the fraction of the candidate space which static GRYFFIN explores to locate the optimum in dependence of the number of categorical variables in the optimization task. For this benchmark, we set up each categorical variable with a total of 11 options and gradually increase the dimensionality of the search space. Fig. S.15 illustrates the performance of static GRYFFIN on different benchmark surfaces with varying dimensionality for a total of 100 independent executions. Descriptors were provided in the reference ordering introduced in Sec. S.2.

We observe that the fraction of the space explored by static GRYFFIN on average decreases with the dimensionality across all benchmark surfaces. More specifically, we find that the dependence of the explored space to the number of parameters can be approximated with an exponential decay of the form  $y = \alpha \exp(-\gamma x)$  where  $y$  denotes the fraction of the explored space,  $x$  denotes the number of parameters and  $\alpha$  and  $\gamma$  are two parameters which we infer from a least-square fit. Parameter values are reported in Tab. S.2.



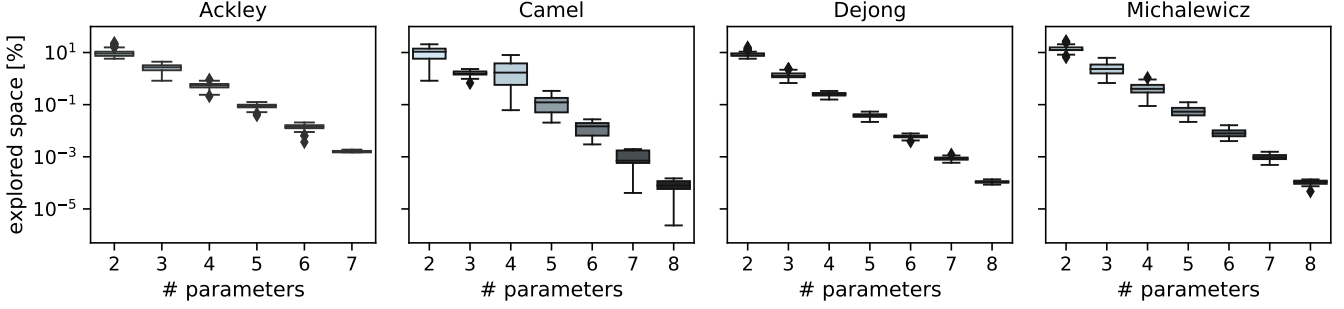


FIG. S.14: Fraction of explored space required by static GRYFFIN to locate the optimum for varying dimensionalities of different benchmark surfaces.

Surface	$\alpha$	$\gamma$	$r^2$	score
Ackley	3.34	1.66	0.84	
Camel	5.26	1.83	0.67	
Dejong	3.86	1.86	0.95	
Michalewicz	8.17	1.95	0.90	

TABLE S.1: Fitting parameters for the dependency of the fraction of the explored space on the number of categorical parameters. The  $r^2$  score indicates the coefficient of determination

This observation indicates that GRYFFIN does not suffer from the *curse of dimensionality*, as the number of evaluated candidates does not increase as fast as the volume of the space.

#### D. Influence of the number of options

We empirically estimate the fraction of the candidate space which static GRYFFIN explores to locate the optimum in dependence of the number of options per categorical variable. For this benchmark, we set up each benchmark surface with two categorical variables and gradually increase the number of options. Fig. S.15 illustrates the performance of static GRYFFIN on different benchmark surfaces with varying options for a total of 100 independent executions. Descriptors were provided in the reference ordering introduced in Sec. S.2.

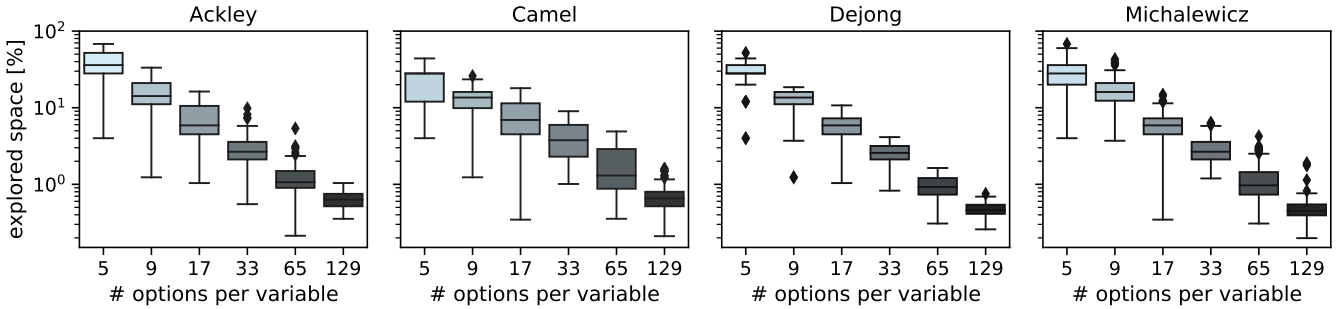


FIG. S.15: Fraction of explored space required by static GRYFFIN to locate the optimum depending on the number of options per parameter for different benchmark surfaces. Note, that the abscissa is not linear.

We observe that the fraction of the space that static GRYFFIN explores to locate the optimum consistently decreases with an increasing number of options across all benchmark surfaces. More specifically, we find that the dependence of the explored space to the number of parameters can be approximated with an exponential decay of the form  $y = \alpha x^{-\gamma}$  where  $y$  denotes the fraction of the explored space,  $x$  denotes the number of options and  $\alpha$  and  $\gamma$  are two parameters which we infer from a least-square fit. Parameter values are reported in Tab. S.2.

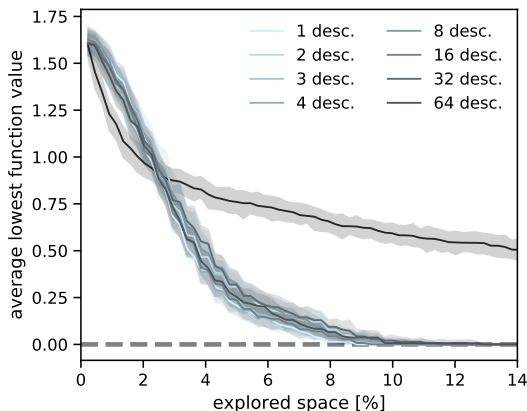
Surface	$\alpha$	$\gamma$	$r^2$	score
Ackley	2.34	1.25	0.73	
Camel	1.20	1.05	0.68	
Dejong	2.04	1.27	0.89	
Michalewicz	2.12	1.25	0.70	

TABLE S.2: Fitting parameters for the dependency of the fraction of the explored space on the number of categorical parameters. The  $r^2$  score indicates the coefficient of determination

### E. Influence of the number of descriptors

Static GRYFFIN facilitates the acceleration of categorical optimization by supplying an arbitrary number of real valued descriptors for every option of the categorical variable. This benchmark investigates the performance of GRYFFIN when changing the number of descriptors which construct the same metric space, while keeping the information content of the descriptors constant. Simulations are run on the *michalewicz* surface (see Sec. S.2) with two categorical variables and 21 options per variable. Descriptors are constructed for the reference ordering and repeated multiple times to span the same metric space. Optimization runs are repeated 100 times with different random seeds to marginalize performance fluctuations.

A) Optimization traces



B) Fractions of the explored space

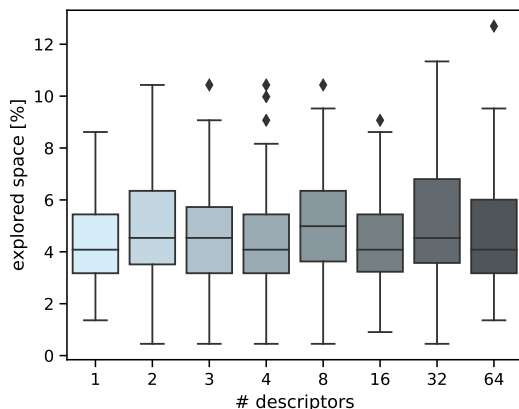


FIG. S.16: Performance of GRYFFIN with varying number of descriptors spanning the same metric space shown on the *michalewicz* surface in reference ordering. Optimization runs have been repeated 100 times with different random seeds. Panel (A): Achieved best function values in dependence of the explored fraction of the search space. The performance of a random search is shown for reference. Panel (B): Fraction of the search space which had been evaluated when the optimal parameter combination was detected for different numbers of descriptors.

Overall, we find very similar performances across the different numbers of descriptors. Both the explored fraction of the space when detecting the optimum (Fig. S.16b) and the traces of best values achieved during the optimization (Fig. S.16a) do not display any significant differences. We conclude that the performance does not depend on the number of provided descriptors provided the descriptors encode the same information.

## S.4. REAL-WORLD APPLICATIONS OF GRYFFIN

Following the empirical benchmarks of GRYFFIN on synthetic functions (see Sec. S.3) we demonstrate its applicability on three real-world examples: the discovery of non-fullerene acceptors for organic solar cells, (ii) the discovery of hybrid organic-inorganic perovskites, and (iii) the optimization of reaction conditions for Suzuki-Miyaura cross-coupling reactions. Datasets for all three applications are made available on GitHub.<sup>9</sup>

### A. Non-fullerene acceptors

The discovery task on non-fullerene acceptors involves the selection of molecular fragments which are assembled to non-fullerene acceptor candidates for solar cell applications, following a recent study by Lopez *et al.*<sup>10</sup> We consider a

subset of the publicly available library with 4,216 acceptor candidates assembled from the following fragments:

- Terminal fragments: frag\_31, frag\_32, frag\_33, frag\_34, frag\_36, frag\_38, frag\_47, frag\_49, frag\_51, frag\_52, frag\_63, frag\_64, frag\_68, frag\_72, frag\_114, frag\_115, frag\_119
- Core fragments: frag\_1, frag\_2, frag\_3, frag\_23, frag\_88, frag\_98, frag\_107, frag\_109
- Spacer fragments: frag\_4, frag\_5, frag\_6, frag\_7, frag\_14, frag\_17, frag\_19, frag\_22, frag\_24, frag\_25, frag\_46, frag\_55, frag\_57, frag\_58, frag\_60, frag\_61, frag\_81, frag\_82, frag\_85, frag\_90, frag\_100, frag\_101, frag\_105, frag\_108, frag\_110, frag\_112, frag\_120, frag\_121, frag\_127, frag\_128, frag\_129

All fragments are characterized by a set of three electronic properties (HOMO and LUMO levels and the dipole moment) which are computed at the B3LYP/Def2SVP level of theory on a SuperFineGrid using Gaussian,<sup>11</sup> and two geometric properties (molecular weight and radius of gyration) which were computed for the ground state geometry. Since the optimization targets for all 4,216 candidates have been tabulated by Lopez *et al.*,<sup>10</sup> we can compute the correlation of every descriptor with the optimization targets. Results are reported in Tab. S.3, where we find that the electronic properties collectively correlate best with the optimization targets (although correlations are relatively poor overall).

	Core	Spacer	Terminus
HOMO	0.073	-0.022	<b>-0.080</b>
LUMO	<b>-0.276</b>	-0.171	-0.075
Dipole moment	-0.220	<b>0.199</b>	-0.019
Molecular weight	0.199	-0.003	-0.056
Radius of gyration	0.075	-0.038	0.048

TABLE S.3: Correlations of physical descriptors with observed performances of individual choices for termini, spacer and cores. Highest correlations are printed in bold.

Fig. S.17 illustrates the performances of the studied optimization strategies on the non-fullerene application described in detail in Sec. V.A. Each candidate molecule is assigned a rank based on its power conversion efficiency, starting from 1 for candidate with the highest power conversion efficiency up to 4,216 for the candidate with the lowest power conversion efficiency. The graphs shown in Fig. S.17 illustrate the average rank of the best performing candidate for different stages of 200 independent optimization runs.

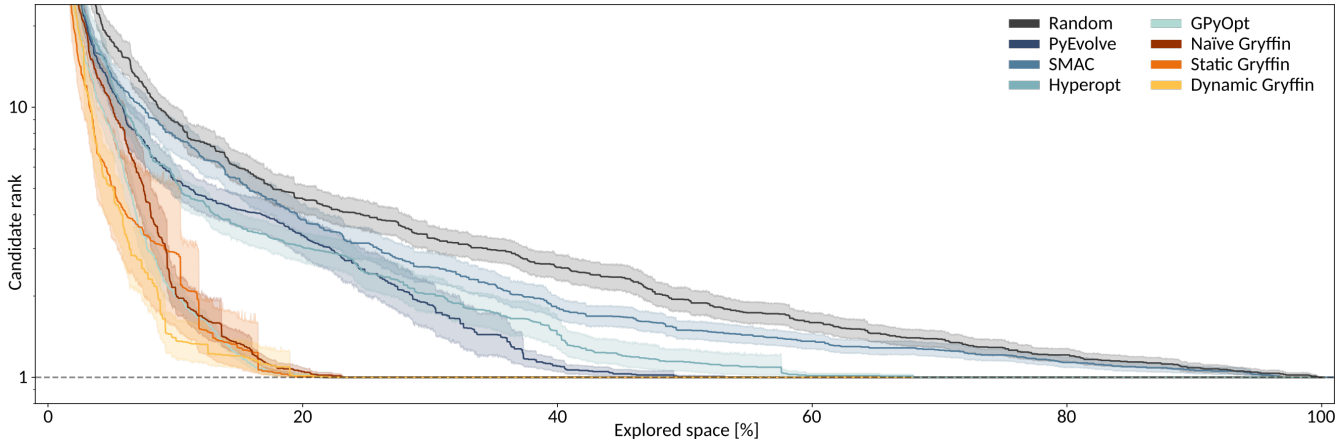


FIG. S.17: Average rank of the candidate with the highest power conversion efficiency identified by the different optimization strategies during 100 independent optimization runs.

In agreement with the results reported in Sec. V.A we observe that the dynamic formulation of GRYFFIN locates promising candidates the fastest. While static GRYFFIN initially also shows a promising optimization rate, identifying candidates in the top 10 ranks with less than 10 % of the space explored, it noticeably slows down compared to the dynamic and even the naïve formulations, indicating that the provided descriptors might not directly favor the best performing candidate. This observation agrees with the fact that the descriptors overall correlate poorly with the optimization targets.

### B. Hybrid organic inorganic perovskites

We construct hybrid organic-inorganic perovskites (HOIP) from a set of different options for the inorganic cation, the inorganic anion and the organic anion. HOIP designs are evaluated based on their bandgap, and ranked from lowest to highest. Inorganic constituents are characterized by their electron affinity, ionization energy, total mass and electronegativity. Organic anions are described by a set of electronic properties (HOMO, LUMO, dipole moment, atomization energy) and geometric properties (radius of gyration, molecular weight). Correlations between individual descriptors and the computed HOIP bandgaps are reported in Tab. S.4

	Inorganic anion		Organic anion	
	Inorganic anion	Inorganic cation	HOMO	LUMO
Electron affinity	0.452	-0.116	0.002	0.140
Ionization energy	<b>0.904</b>	0.121	Dipole moment	0.077
Total mass	-0.804	0.069	Atomization energy	<b>-0.159</b>
Electronegativity	0.902	<b>0.142</b>	Radius of gyration	0.145
			Molecular weight	0.138

TABLE S.4: Correlations of physical descriptors with observed performances of individual choices for termini, spacer and cores. Largest correlation magnitudes are printed in bold.

Fig. S.18 illustrates the performances of the studied optimization strategies on the perovskite application described in detail in Sec. V.B. Each perovskite candidate is assigned a rank based on its bandgap efficiency, starting from 1 for candidate with the lowest bandgap up to 192 for the candidate with the highest bandgap. The graphs shown in Fig. S.18 illustrate the average rank of the best performing candidate for different stages of 200 independent optimization runs.

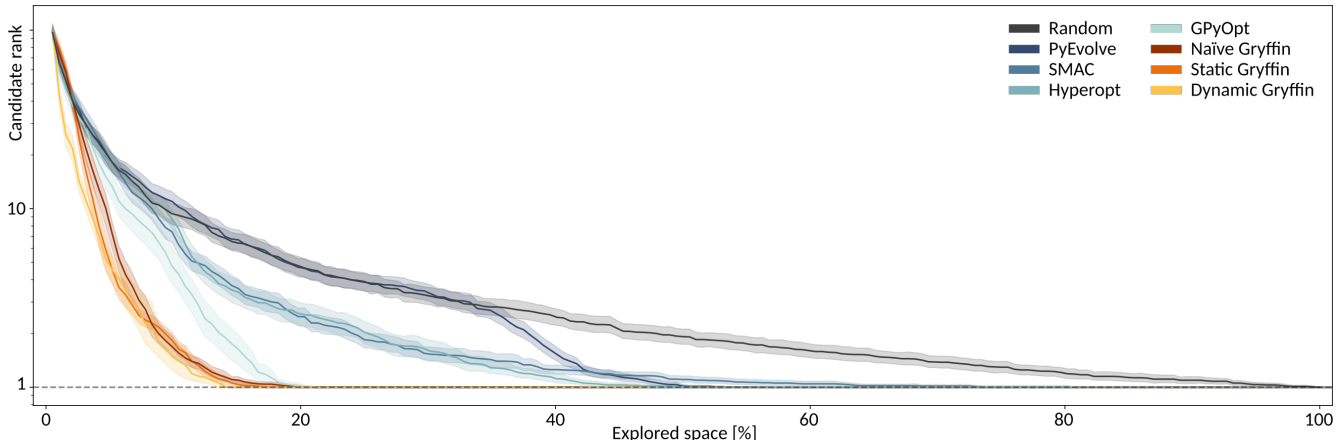


FIG. S.18: Average rank of the candidate with the lowest bandgap identified by the different optimization strategies during 100 independent optimization runs.

In agreement with the results reported in Sec. V.A we observe that the dynamic formulation of GRYFFIN locates promising candidates the fastest. The tendency of static GRYFFIN to show a reduced optimization rate beyond the initial phase as observed for the non-fullerene application (see Sec. S.4.A) is not as prevalent in this application.

### C. Emulating Suzuki-Miyaura cross-coupling reactions

We further demonstrate that GRYFFIN can be used to determine reaction conditions for Suzuki-Miyaura cross-coupling reactions (see Sec. V.C). Specifically, four controllable reaction parameters are defined, following an experimental procedure detailed by Reizman *et al.*:<sup>12</sup> the reaction temperature, the residence time, the catalyst loading and the ligand are selected with the goal to maximize the turn-over number (TON) while keeping the reaction yield at acceptable levels ( $> 85.4\%$ ). The acceptance threshold for the reaction yield is inspired by the experimental results reported in Ref.<sup>12</sup> We considered a temperature between  $30^\circ\text{C}$  and  $110^\circ\text{C}$ , a residence time between 1 min and 10 min

and a catalyst loading between 0.5 % and 2.5 %. We further selected one of seven ligands, which are described in more detail in the main text (see Sec. V.C).

Repeated executions of individual experiments are avoided by constructing an emulator of the experimental procedure based on previous measurements using a probabilistic machine learning model. The probabilistic model has the potential to reproduce and interpolate measurements obtained from previous experiments, which allows to query the experimental response for any parameter combination via the trained probabilistic model without the need to run additional experiments, as previously demonstrated in the context of the auto-calibration of high-performance liquid chromatography equipment.<sup>13</sup>

### 1. Constructing an experiment emulator

Reizman *et al.* report the reaction yield and TON for a total of 88 Suzuki-Miyaura cross-coupling reactions,<sup>12</sup> which are used to train a Bayesian neural network (BNN) as a probabilistic model to predict the reaction yield and the TON for any combination of experimental parameters within the search domain. Since BNNs are probabilistic machine learning models, they have the ability to implicitly infer the degree of experimental noise in addition to the expected average response from the presented dataset.

From the total dataset comprising 88 reactions, eight reactions were separated for the test set. The reactions for the test set were chosen randomly, but with the constraint that each of the seven ligands was used in at least one of the test set reactions. The remaining 80 reactions were used for 10-fold cross-validation. The different ligands were represented as one-hot encoded vectors, and all other experimental conditions were standardized. Both reaction yields and TON were chosen as prediction targets. To account for the fact that both reaction yields and TON cannot be negative, we applied the ReLU activation function to the last layer. Accordingly, the targets were rescaled by dividing by the average reaction yield and TON respectively to simplify the initialization of the BNN. We use leaky ReLUs for all other activations and apply dropout at a rate of 0.1 for further regularization. Distributions for weights and biases are initialized as standard normal distributions. The BNN is constructed with three hidden layers and 24 neurons per layer. Network parameters are inferred via variational inference using the Adam optimization algorithm with an initial learning rate of  $10^{-3}$ .

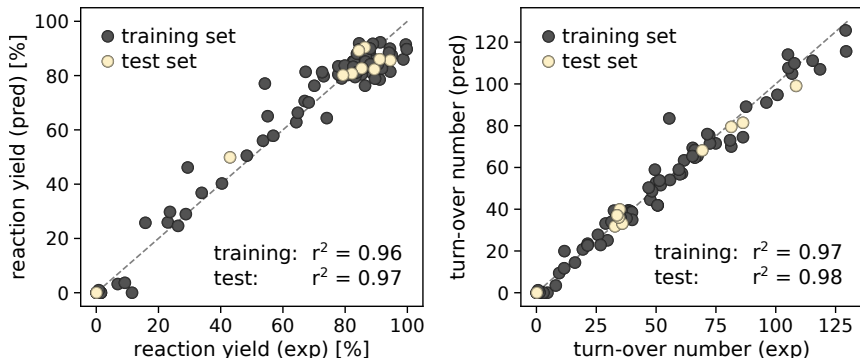


FIG. S.19: Scatter plot of the emulator predictions for the Suzuki coupling.

Scatter plots of the obtained predictions as well as coefficients of determination are illustrated in Fig. S.19. The predicted reactions yields and TONs agree well with the targeted values, which indicates that the trained BNN accurately reproduces the experimental response surfaces of the studied Suzuki-Miyaura reactions.

### 2. Analysis of ligand descriptors

The optimization runs with static and dynamic GRYFFIN are guided by a set of physicochemical descriptors for each of the ligands. Descriptors were chosen based on their availability and computed with RDKit.<sup>14</sup> Descriptor values for each of the ligand choices are illustrated in Fig. S.20

We compute the maximum and average TONs for each ligand on a grid of 100 equidistant levels for each of the three remaining process conditions (temperature, residence time, catalyst loading) and report the results in Tab. S.6. We observe that ligand L3 shows the highest maximum TON and ligand L1 shows the highest maximum yield, while the highest average turnover numbers and yields are achieved with ligand L2.

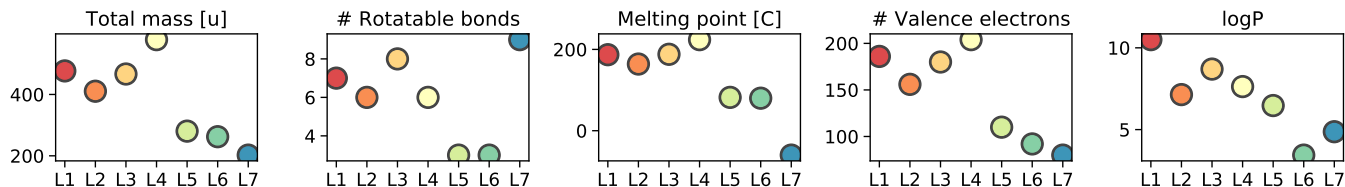


FIG. S.20: Values of the physical descriptors assigned to the individual ligands (L1-L7) to guide static and dynamic GRYFFIN for maximization of the reaction yield and the turnover number of the controlled Suzuki reaction.

	Max TON	Average TON	Max yield [%]	Average yield [%]
L1	129.3	45.1	<b>96.3</b>	59.7
L2	111.8	<b>46.8</b>	95.3	<b>64.3</b>
L3	<b>132.5</b>	45.1	92.7	59.2
L4	62.4	17.7	88.1	28.3
L5	76.3	7.5	62.5	10.5
L6	47.1	3.5	39.9	5.4
L7	52.6	3.3	41.2	4.9

TABLE S.5: Maximum and average turnover numbers (TON) and reaction yields achieved by each ligand on a grid of 100 levels for each of the remaining three process conditions (temperature, residence time, catalyst loading). Highest TONs and yields across all ligands are indicated in bold.

We also analyze the correlation of the provided descriptors with the maximum and average TONs and yields and report the results in Tab. S.6. The logP values of all ligands correlate the best with the maximum TON and the average turnover number and yield, while the number of valence electrons is most indicative of the maximum achievable yield. Given that the first optimization target is a maximization of the reaction yield, the number of valence electrons is expected to be most informative in the initial phase of the optimization. During the optimization, GRYFFIN will favor an more in-depth investigation of the performance of the more promising ligands, such that the number of valence electrons might be considered to be more informative than logP overall.

	Max TON	Average TON	Max yield [%]	Average yield [%]
Molecular weight	0.527	0.649	0.873	0.685
Rotatable bonds	0.361	0.390	0.278	0.385
Melting point	0.592	0.690	0.866	0.718
Valence electrons	0.634	0.729	<b>0.923</b>	0.759
logP	<b>0.847</b>	<b>0.805</b>	0.892	<b>0.806</b>

TABLE S.6: Pearson correlation coefficients between individual ligand descriptors and properties of interest. Largest correlations are printed in bold.

We further compute the pairwise correlations between the provided descriptors and find, that the number of valence electrons, the melting point and the molecular weight generally correlate well with one another. Detailed results are reported in Tab. S.7.

- 
- [1] Florian Häse, Loïc M Roch, Christoph Kreisbeck, and Alán Aspuru-Guzik. Phoenix: A bayesian optimizer for chemistry. *ACS central science*, 4(9):1134–1145, 2018.
  - [2] Diederik P Kingma and Max Welling. Auto-encoding variational bayes. *arXiv preprint arXiv:1312.6114*, 2013.
  - [3] Chris J Maddison, Andriy Mnih, and Yee Whye Teh. The concrete distribution: A continuous relaxation of discrete random variables. *arXiv preprint arXiv:1611.00712*, 2016.
  - [4] Eric Jang, Shixiang Gu, and Ben Poole. Categorical reparameterization with gumbel-softmax. *arXiv preprint arXiv:1611.01144*, 2016.
  - [5] Roger Fletcher. Practical methods of optimization john wiley & sons. *New York*, 80:4, 1987.
  - [6] Florian Häse, Ignacio Fdez Galván, Alán Aspuru-Guzik, Roland Lindh, and Morgane Vacher. How machine learning can assist the interpretation of ab initio molecular dynamics simulations and conceptual understanding of chemistry. *Chemical*

	Molecular weight	Rotatable bonds	Melting point	Valence electrons	logP
Molecular weight	1.00	0.20	0.93	0.99	0.76
Rotatable bonds	0.20	1.00	-0.08	0.26	0.39
Melting point	0.93	-0.08	1.00	0.93	0.70
Valence electrons	0.99	0.26	0.93	1.00	0.84
logP	0.76	0.39	0.70	0.84	1.00

TABLE S.7: Pairwise Pearson correlation between physical descriptors of individual ligands.

*Science*, 10(8):2298–2307, 2019.

- [7] Ronald A Fisher. Frequency distribution of the values of the correlation coefficient in samples from an indefinitely large population. *Biometrika*, 10(4):507–521, 1915.
- [8] Ronald A Fisher. On the 'probable error' of a coefficient of correlation deduced from a small sample. *Metron*, 1:1–32, 1921.
- [9] F. Häse, L. M. Roch, and A. Aspuru-Guzik. Gryffin: An algorithm for bayesian optimization for categorical variables informed by physical intuition with applications to chemistry. *GitHub*, <https://github.com/aspuru-guzik-group/gryffin>, 2019.
- [10] Steven A Lopez, Benjamin Sanchez-Lengeling, Julio de Goes Soares, and Alan Aspuru-Guzik. Design principles and top non-fullerene acceptor candidates for organic photovoltaics. *Joule*, 1(4):857–870, 2017.
- [11] M. J. Frisch, G. W. Trucks, H. B. Schlegel, G. E. Scuseria, M. A. Robb, J. R. Cheeseman, G. Scalmani, V. Barone, G. A. Petersson, H. Nakatsuji, X. Li, M. Caricato, A. V. Marenich, J. Bloino, B. G. Janesko, R. Gomperts, B. Mennucci, H. P. Hratchian, J. V. Ortiz, A. F. Izmaylov, J. L. Sonnenberg, D. Williams-Young, F. Ding, F. Lipparini, F. Egidi, J. Goings, B. Peng, A. Petrone, T. Henderson, D. Ranasinghe, V. G. Zakrzewski, J. Gao, N. Rega, G. Zheng, W. Liang, M. Hada, M. Ehara, K. Toyota, R. Fukuda, J. Hasegawa, M. Ishida, T. Nakajima, Y. Honda, O. Kitao, H. Nakai, T. Vreven, K. Throssell, J. A. Montgomery, Jr., J. E. Peralta, F. Ogliaro, M. J. Bearpark, J. J. Heyd, E. N. Brothers, K. N. Kudin, V. N. Staroverov, T. A. Keith, R. Kobayashi, J. Normand, K. Raghavachari, A. P. Rendell, J. C. Burant, S. S. Iyengar, J. Tomasi, M. Cossi, J. M. Millam, M. Klene, C. Adamo, R. Cammi, J. W. Ochterski, R. L. Martin, K. Morokuma, O. Farkas, J. B. Foresman, and D. J. Fox. Gaussian16 Revision C.01, 2016. Gaussian Inc. Wallingford CT.
- [12] Brandon J Reizman, Yi-Ming Wang, Stephen L Buchwald, and Klavs F Jensen. Suzuki–miyaura cross-coupling optimization enabled by automated feedback. *Reaction chemistry & engineering*, 1(6):658–666, 2016.
- [13] Florian Häse, Loïc M Roch, and Alán Aspuru-Guzik. Chimera: enabling hierarchy based multi-objective optimization for self-driving laboratories. *Chemical Science*, 9(39):7642–7655, 2018.
- [14] Greg Landrum et al. Rdkit: Open-source cheminformatics. 2006.